Experimental validation of a numerical knee model

Schoonen, J.F.M.

Award date:
1993

Experimental validation of a numerical knee model

by: J.F.M. Schoonen

W.F.W.93.087

Professor	:	Prof. Dr. Ir. J.D. Janssen
Coaches	:	Dr. Ir. C.W.J. Oomens
		Ir. M.A.M. van Lankveld

Eindhoven, July 1993
Eindhoven University of Technology
Department of Mechanical Engineering
Division of Fundamentals

Summary

In the study here presented, both experiments and numerical analyses have been performed on a model of the human knee contact. The model has a simple geometry and contains the following elements: tibial articular cartilage layer, femoral bony end and in between the meniscus. The bony end is considered rigid and impervious, whereas cartilage layer and meniscus are modelled as mixtures, consisting of a solid and a fluid phase.

The main goal of this study is the verification of the numerical mixture modelling. Therefore an experimental set-up has been developed in order to apply a load to the physical model and to measure several pressures and displacements. Porous polyurethane is used for the solid phase and an oil for the fluid phase of the mixture components. A total of four configurations have been tested, which differ from each other with respect to the presence of the meniscus and its material properties.

Both in experiments and numerical calculations, the presence of the meniscus gives considerable changes in the response of the model. The indentation as well as the pressures become much lower and a more equal distribution of the pressure is found.

In the confrontation between numerical and experimental results qualitative as well as quantitative agreements are found. There are also some differences, but these probably can be ascribed to the more complex material behaviour of meniscus and disc in the experiments.

The results of this study therefore indicate the validity of the numerical mixture formulation.

Contents

References

Appendices

A Resultaten Metingen

B Verplaatsing Meniscus

C Materiaal Karakterisatie

D Apparatuur

E Calibratie Curves

F DIANA Programma's

1. Introduction

The knee is one of the most complex and heavily loaded joints in the human body. It is subjected to many injuries and diseases, for instance osteoarthritis and rheumatoid arthritis, which are both frequently occuring chronical affections. Most of the surgical and non-surgical interventions performed are based on clinical experiences rather than on fundamental understanding. From different points of view, therefore it is tried to obtain more insight into the functions of, and interactions between the different parts of the knee joint. One way of doing this is by describing the joint with a mathematical model. Because modelling the whole joint is too difficult for the time being, studies are concentrated on sub-connections. When more insight into the different sub-connections has been achieved, these can be integrated into a model of the complete joint.

1.1 The Knee Contact

The tibial-femoral contact is central to this study and the relevant elements are: the bony ends of femur and tibia, their articular cartilage layers and menisci. These elements are indicated in Figure 1, which shows a cross section of the knee joint.

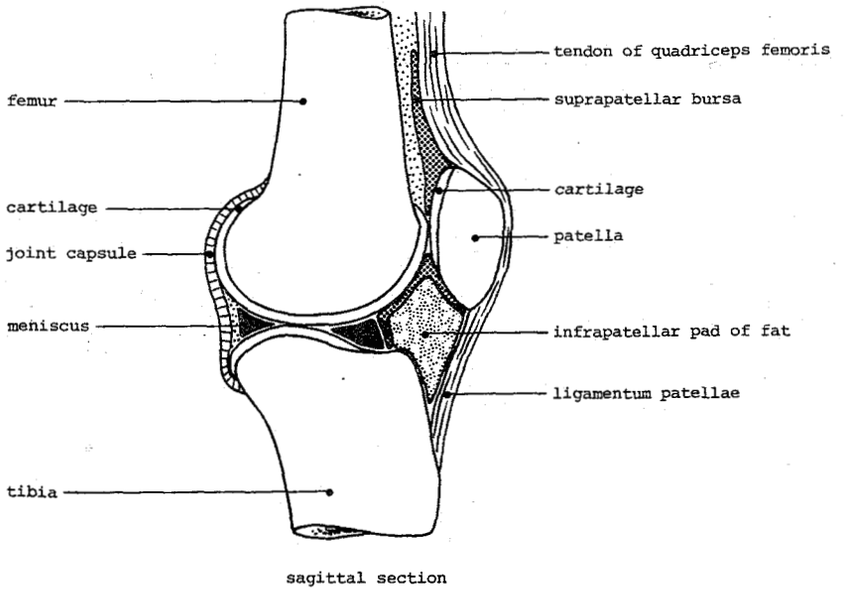

Figure 1: *Cross section of the human knee joint.*

The ends of femur and tibia consist of two condyles, covered by layers of articular cartilage. Motion of the joint takes place along these layers in a environment of synovial fluid. The surfaces of the condyles are incongruent, but the space in between is fairly well filled by the menisci. As can be seen in Figure 2 the menisci are semi lunar shaped and fixed to the centre of the tibial surface.

Both articular cartilage layers and menisci consist of a solid organic matrix, predominantly composed of collagen fibers and proteoglycan macro-molecules, which is filled with a viscous fluid, predominantly water. In mechanical terms they can be described as multi-phase nonlinear permeable anisotropic viscoelastic materials. The time dependent and viscous effects of the bony components can be considered very small.

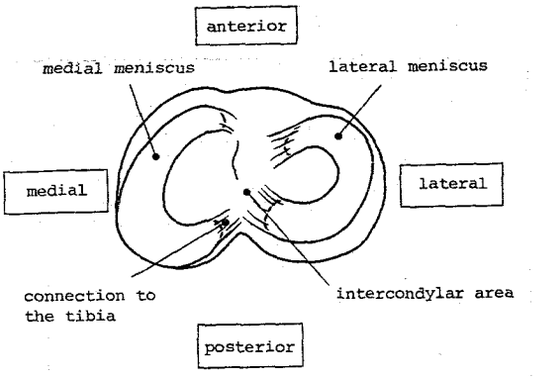

Figure 2: *Top view of menisci and tibial surface.*

1.2 Modelling

Schreppers [1] developed an axisymmetric model to investigate the force transmission through the tibial-femoral contact, both direct via cartilage layers and indirect via menisci. He followed a stepwise modelling approach; during each step parameter studies were performed in order to investigate the functions of the relevant components. He started with a geometrically nonlinear model consisting of bony ends, cartilage layers and meniscus. The materials of the different components were modelled with a linear relation between the second Piola-Kirchoff stresses and the Green-Lagrange strains. Specially developed contact elements were used to allow sliding of the meniscus along the cartilage layers. The relatively soft cartilage layers were found to play an important role in the stress distribution in the direct contact area, whereas the deformations of the bony ends could be neglected.

In the next step cartilage layer and meniscus were modelled as mixtures (Oomens [2]). They consisted of a solid and a fluid phase, fluid transport between cartilage layer and meniscus was possible. When the fluid could flow freely out of the model, the load distribution changed enormously in time.

This modelling stategy is continued by van Lankveld. A more realistic, but still axisymmetric, geometry has been chosen as can be seen in Figure 3. The model consists of one cartilage layer and meniscus, both modelled as mixtures. The influence of nonlinear elastic behaviour of the solid constituent and the anisotropic behaviour of the meniscus is examined. Also parameter studies are performed to investigate the influence of material

properties.

The mathematical equations, involved with mixture modelling, contain a number of physical assumptions. Solid and fluid phase for instance are considered to be intrinsically incompressible, while gravity and inertia forces are neglected. In the numerical formulation discretization of the equations occurs and an iterative solution method is necessary. Also special elements are needed to describe contact between mixtures and/or solid systems, again introducing assumptions and estimations. The results of the numerical modelling, therefore, are not obvious and should be validated with experiments.

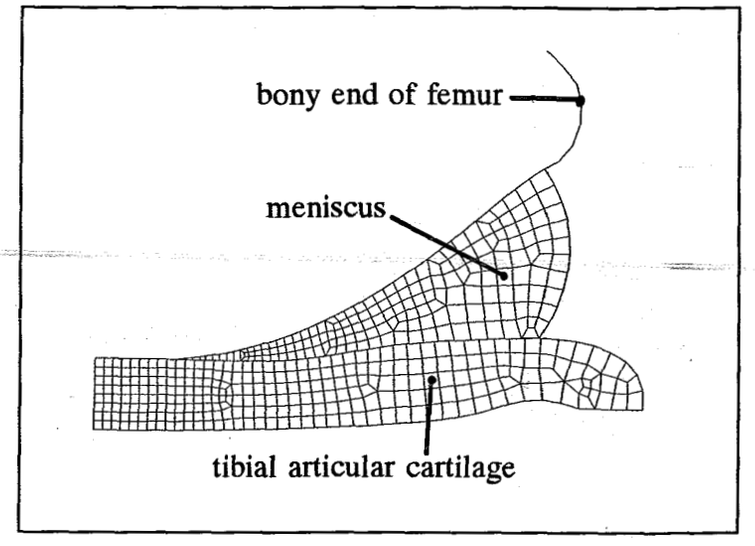

Figure 3: *FE-model of the knee contact.*

1.3 Objective

In this study a numerical model of the knee contact is physically realized and tested. The model has a simple geometry, resembling the reduced model of Schreppers, and comprises one deformable cartilage layer, a rigid indentor and a meniscal ring. Layer and meniscus are modelled as mixtures, while indentor is a single phase solid.
The goal of the study is twofold. First of all it is investigated if the numerical formulation gives a good approximation of the physical mixture model. Secondly the influence will be examined of the meniscus and its properties.
Meniscus and articular cartilage are made of porous polyurethane and an oil is used as fluid phase. In an experimental set-up a quasistatic load is applied and several pressures and the displacement of the indentor are measured as a function of time. To investigate the influence of the meniscus, experiments are performed without meniscus as well as with three different ones. Experimental model, set-up and results will be discussed in chapter 2. With the FE-package DIANA numerical calculations are made for a model with and without meniscus. Chapter 3 gives a description of the FE-model together with the results. After the seperate treatment of experiments and FE-calculations, the numerical results are confronted with the experiments in chapter 4. Finally, the conclusions with respect to this study are given in chapter 5.

2. Experiments on a Physical Model of the Knee

2.1 Model Description

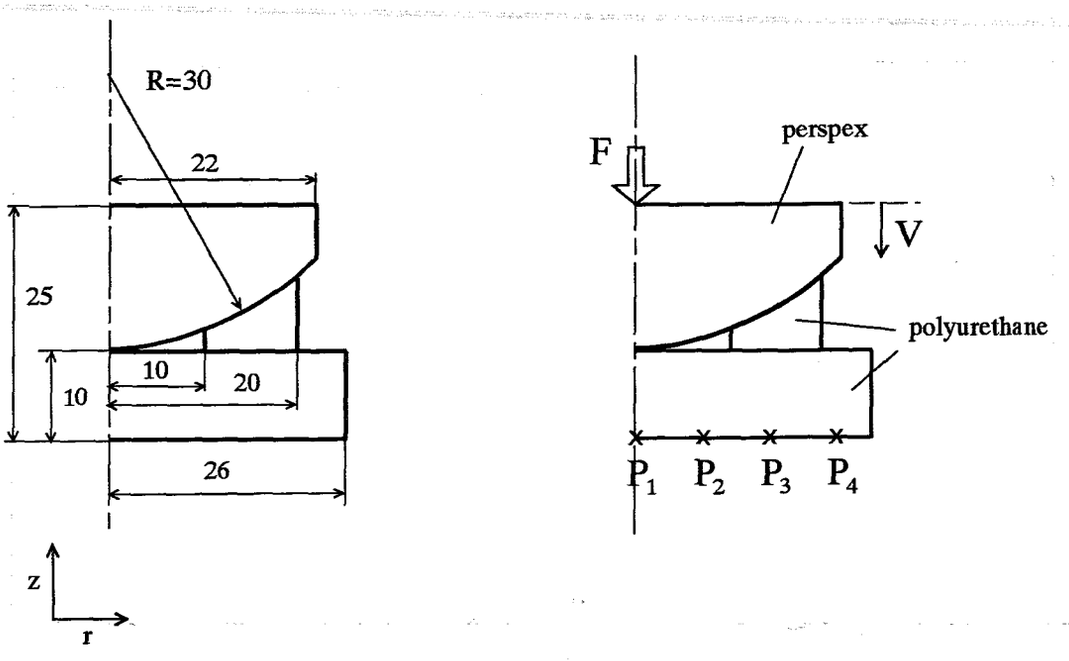

Figure 4a and b: *Half a cross section of the knee model. In 4a the dimensions are given in mm, 4b shows the responses of the model.*

For validation of the numerical calculations a model is chosen based on the reduced model of Schreppers [1]. Figure 4a shows half a cross section of the model with its dimensions. The model is axisymmetric and consists of a flat disc. On top of that is a spherical indentor while the space in between is partially filled by a wedge-shaped ring. The disc, indentor and ring represent the tibial cartilage layer, the bony end of the femur and the meniscus respectively. Disc and meniscus consist of saturated porous material, while the indentor is a stiff single phase solid. The disc rests on a rigid foundation and is loaded, perpendicular to its outer surface, by the indentor.

In Figure 4b the responses of the model are denoted that will be measured and compared with numerical results: 4 pressures at the bottom surface of the disc (P_1 to P_4) and the vertical displacement of the indentor (V). Also indicated in Figure 4b are the materials of which the different components are composed. The indentor is made of perspex, disc and meniscal ring of porous polyurethane.

2.2 Experimental Set-up

The experimental set-up consists of two main parts; the first is a perspex container, developed by Feron [3], for measuring pressures at the bottom of the disc. Secondly a balance arm, for applying the load in a proper way. Both parts are connected by a rigid frame. Figure 5 shows a cross section of the container together with the load balance arm.

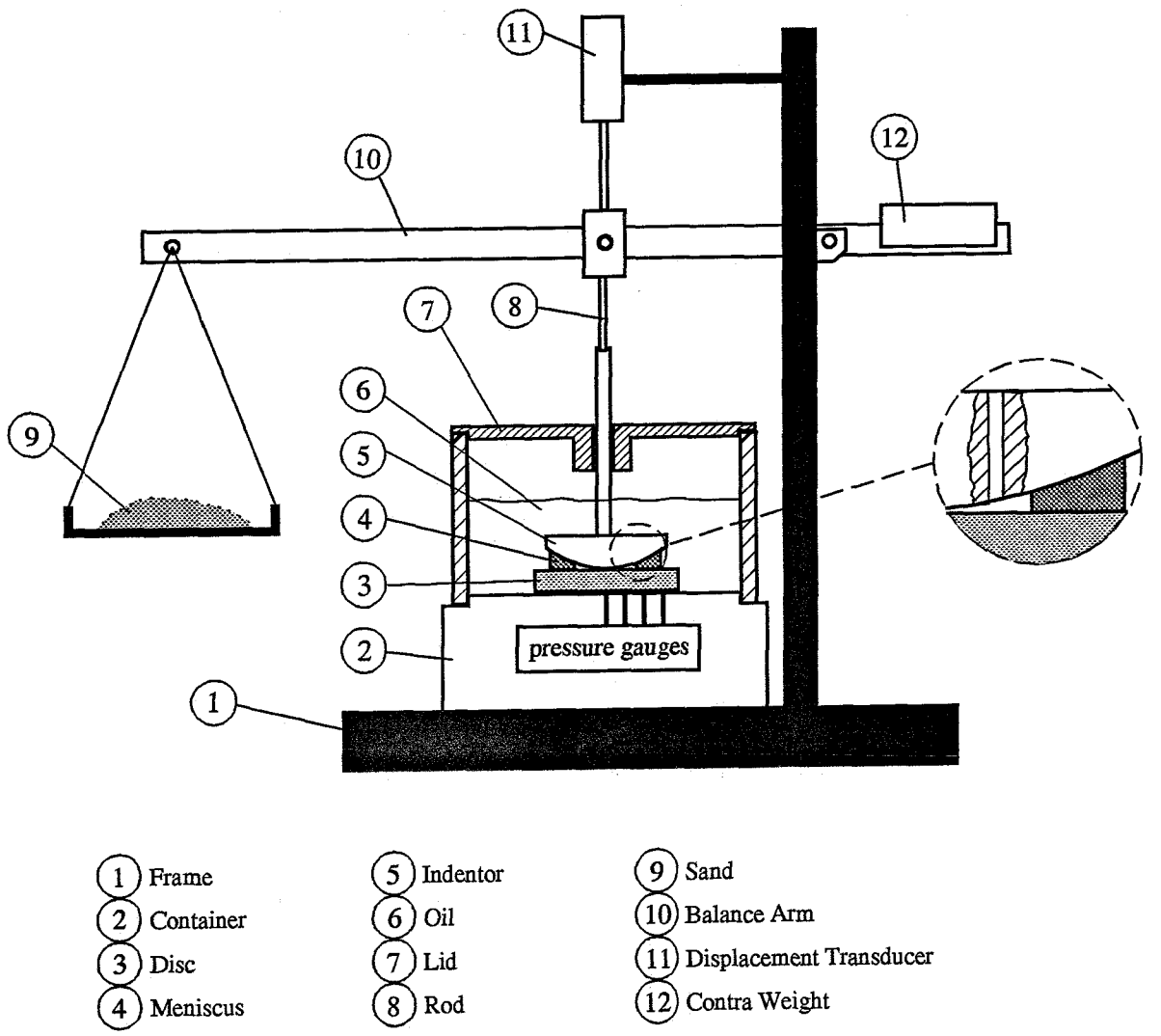

Figure 5: *Cross section of container with model, together with the load balance arm.*

The disc rests on the bottom piece of the container and is centered with a ring. At four different radii, R=0, 7, 14 and 21 mm, small channels are present which are connected with pressure gauges. The spherical indentor, guided by the lid of the container, is pushed down by a rod which is attached to the balance arm. The rod is extended to the top, where its vertical displacement is measured with a displacement transducer (Scheavitz 050DC-D). The whole model is underneath the fluid level.

The load is applied by letting sand stream through a funnel on the load tray of the balance arm. In this way the load is applied gradually and reproducable. When the tray is unloaded, the balance arm is kept horizontal by a contra weight. The fluid in the cavity between disc, indentor and meniscus can flow freely through 8 channels (∅=1mm) in the indentor, shown in the detail of Figure 5.

2.3 Materials

In the experimental model both meniscus and articular cartilage layer are made of synthetic materials, recently developed by de Heus [4]. They are composed of polyurethane on a polyester base (desmopan 8366). First a homogeneous solution is made of polyurethane and diluent in a bath of 80 °C. The solution is casted into the desired shape and cooled to induce crystallization of the diluent. The specimens result after removal of the diluent via solvent extraction. Varying the amount of polymer in the solution (max. 20%) gives materials with different properties.
Three different solutions are used: 10, 15 and 20%. Of each solution a meniscus and a disc (dimensions: 52x10mm) are made. To characterize the materials unconfined compression and permeability tests are performed on the discs. In the compression test strain steps of 2% are applied, after each step the material is relaxed for 270 seconds before stress and strains are calculated.
Besides this characterization of the solid matrix as a linear elastic material also a linear viscoelastic characterization has been performed. A 3-parameter Maxwell chain model is used to describe the viscoelastic behaviour of the 15% disc. The three dimensional relation between stresses and strains is given by:

$$\sigma_{ij}(t) = \int_0^t \left[E_0 + E_1 e^{-\frac{(t-\tau)}{\lambda_1}} \right] D_{ijkl}\, \dot{\varepsilon}_{kl}(\tau)\, d\tau$$

The material behaviour in the compression test can be described with a one dimensional model. This is shown in Figure 6 together with the parameters.
To reduce the permeabilities of the materials a transparant oil (SHELL ONDINA 33) has been taken instead of water as a fluid medium. For the determination of the permeabilities a special apparatus has been constructed.
A more detailed description of the tests is given in Appendix C. The results can be found in Table 1. The Poisson ratio υ is taken from tensile tests performed by Goijaerts [5] on 10% tensile strips. It was found to be υ=0.38 [-].
It should be emphasized that for a full characterization of the materials more complex and time-consuming experiments are required, which was not the objective of this study. Therefore the determined values should be seen as estimations of the real properties. This discrepancy is discerned and addressed to in the modelling strategy.

material	E (MPa)	K (mm^4/Ns)
10%	0.08	510.2
15%	0.25	84.1
20%	0.33	33.2

Table 1: *Values of elastic modulus and permeability resulting from various tests performed on discs (dimensions: 52x10mm).*

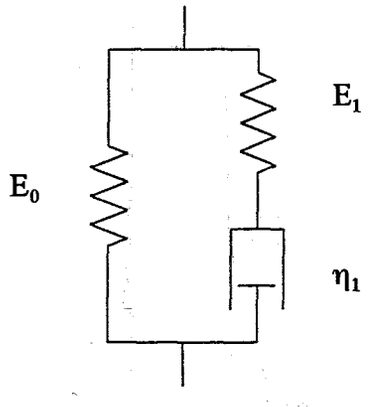

$E_0 = 0.3$ [MPa]

$E_1 = 0.2$ [MPa]

$\lambda_1 = \eta_1/E_1 = 1.7$ [s]

Figure 6: *3-parameter Maxwell chain model used to describe the viscoelastic behaviour of the 15% disc.*

2.4 Experimental Procedures

A total of four different configurations have been tested, summarized in Table 2. As reference configuration both meniscus and disc are made of a 15% solution; model A. To investigate the influence of the meniscus on the load transmission, also tests are performed on models without meniscus and with a meniscus made of a 10% and 20% solution; model B, C and D respectively. The models are made airfree in a vacuum clock.
All the configurations are preloaded by the weight of the indentor (F=0.25 N) and, except for the one without meniscus, an extra load of 1 N to ensure all surfaces touch.
Each configuration is loaded at three levels and each load level is repeated two times. At least twice the loading time is waited after unloading to regain initial conditions. Before the experiments take place the force-time curves are measured with a force transducer, placed halfway the balance arm. As can be seen in Figure 7 the load is not applied with a pure ramp, but the impuls of the falling sand gives an extra load at the end of load appliance. All tests are performed at a temperature of 21,5±1°C.

Model	material meniscus	preload [N]
A	15%	1.25
B	---	0.25
C	10%	1.25
D	20%	1.25

Table 2: *Different configurations with respect to the meniscus (in all configurations the disc was 10mm high and made of a 15% solution).*

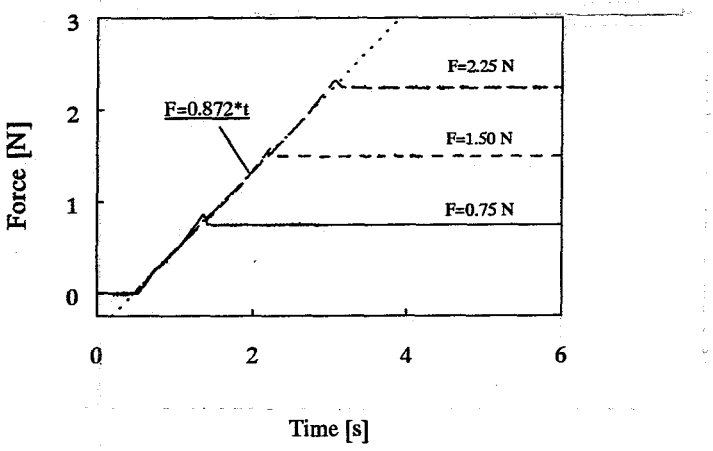

Figure 7: *Force-time curves.*

2.5 Results

For each configuration the results are averaged per load level and can be found in Appendix A (the differences from mean are less than 10%). The measured response of the physical model for the middle load (F=1.5 N) lies in between the two others. The higher load gives higher pressures and indentation of the disc, as for the lower load the opposite is found. The results for the middle load are chosen to compare with numerical analyses and therefore only these are considered in the next paragraphs. First the results for the model with and without meniscus will be discussed. Then the responses are compared of the models with different menisci. At the end of this chapter some concluding remarks will be given.

2.5.1 Model with/without Meniscus

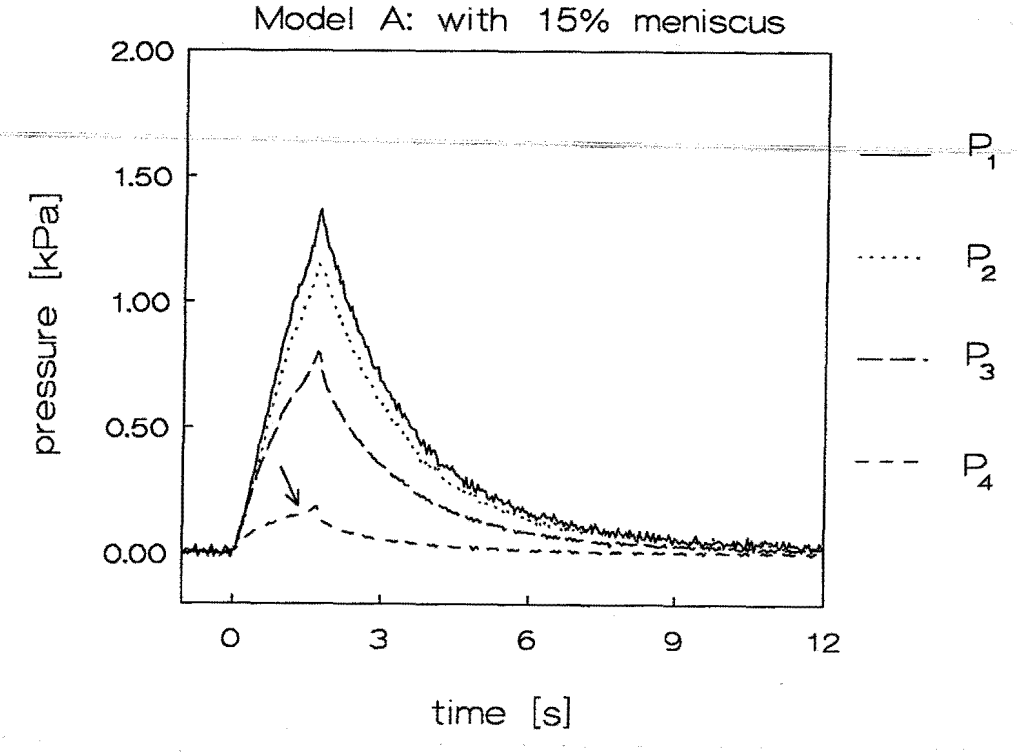

Figure 8: *P_1 to P_4 for model A (with 15% meniscus).*

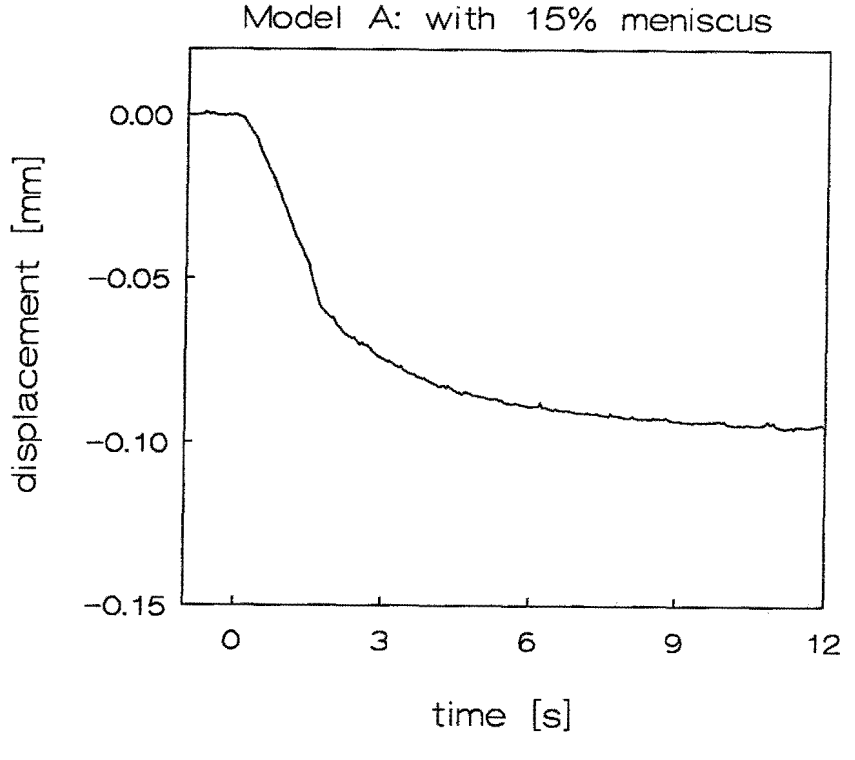

Figure 9: *V for model A (with 15% meniscus).*

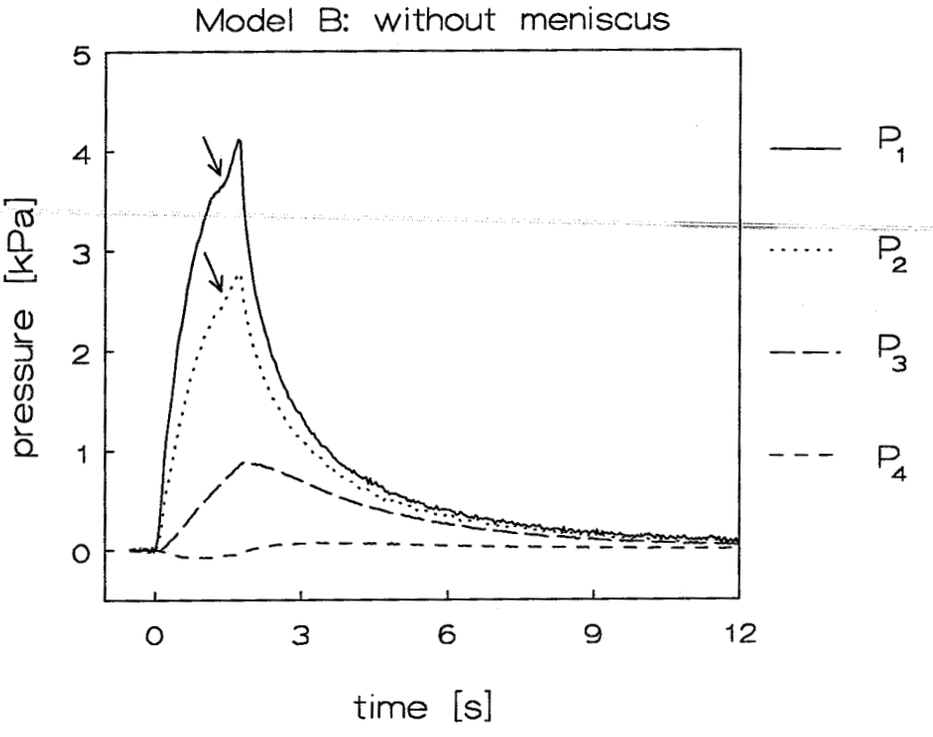

Figure 10: *P_1 to P_4 for model B (without meniscus).*

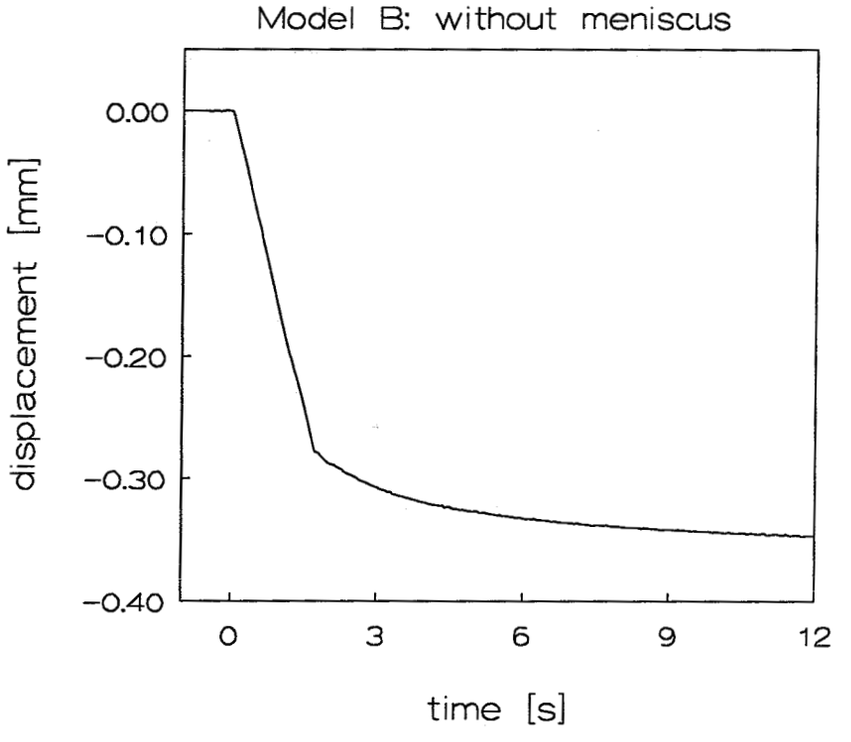

Figure 11: *V for model B (without meniscus).*

Figure 8 and 10 show the measured pressures at the lower surface of the disc (P_1 to P_4), Figure 9 and 11 the displacement of the indentor (V). Both configurations show the

following characteristics:

- When the load is applied (t=0 to 1.72s) pressure is built up in the middle of the disc. Immediately afterwards the pressure drops due to fluid flow out of the disc. The highest pressure is measured in the middle (P_1) and going outward, from P_1 to P_4, a decrease in magnitude of the pressure is found at all times. Around t=10s the pressures become zero and the load will totally be carried by the solid phase only.
- The displacement of the indentor shows to be linearly dependent on time (cq load) during load appliance. Afterwards the movement progresses slowly and even at t=10s the indentor displacement is still increasing. Because the fluid phase does not contribute to the load transmission anymore at that moment, this indicates viscoelastic behaviour of the solid phase.
- The extra load, caused by the impuls of the sand, results in a sudden peak in some of the pressures at t=1.72s, as indicated in Figures 8 and 10 with arrows.

Of course, there are also a number of differences between the two experiments. To investigate the influence of the meniscus' presence on the pressure, a total of 8 parameters may be compared. For sake of clearness this is only done at five times; t=0.8, 1.72, 2.5, 3.5 and 5s also indicated in Figure 12. For these moments the pressures are put next to each other per channel for the two configurations, Figure 13 shows the resulting graph. In this way both a quantitative comparison can be made and the pressure distribution can be investigated. The displacement for the two configurations can be seen in Figure 14.

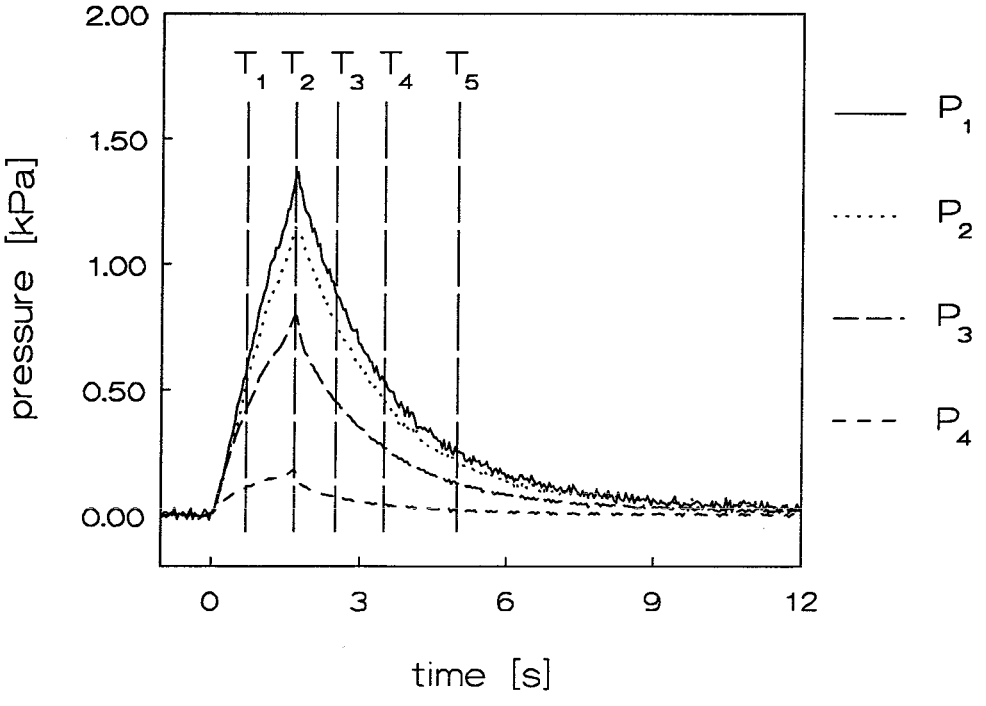

Figure 12: *Moments at which pressure signals are compared: t=0.8, 1.72, 2.5, 3.5 and 5s.*

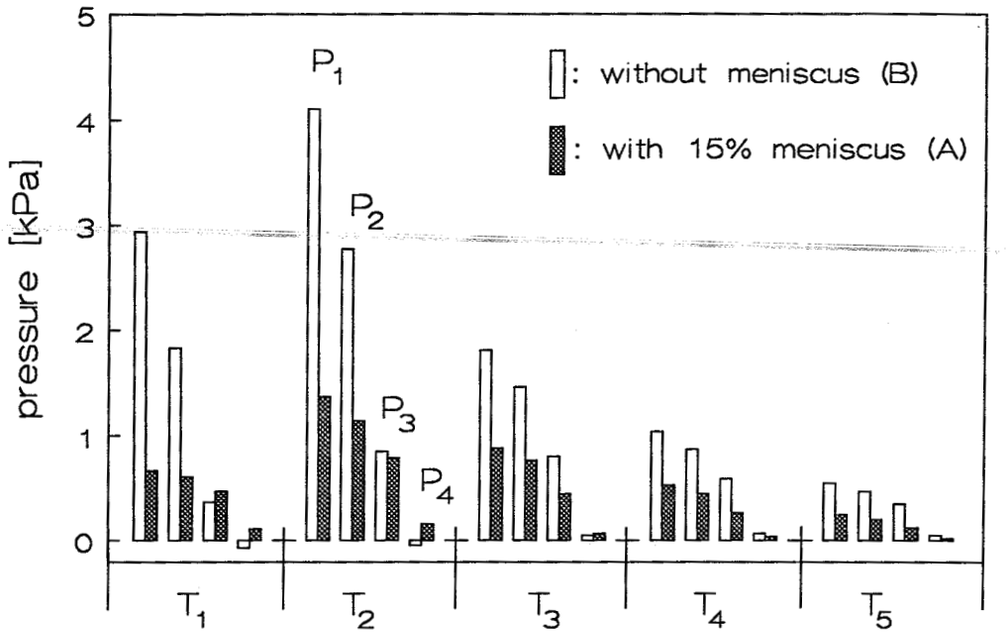

Figure 13: *P_1 to P_4 for model A and B at five times.*

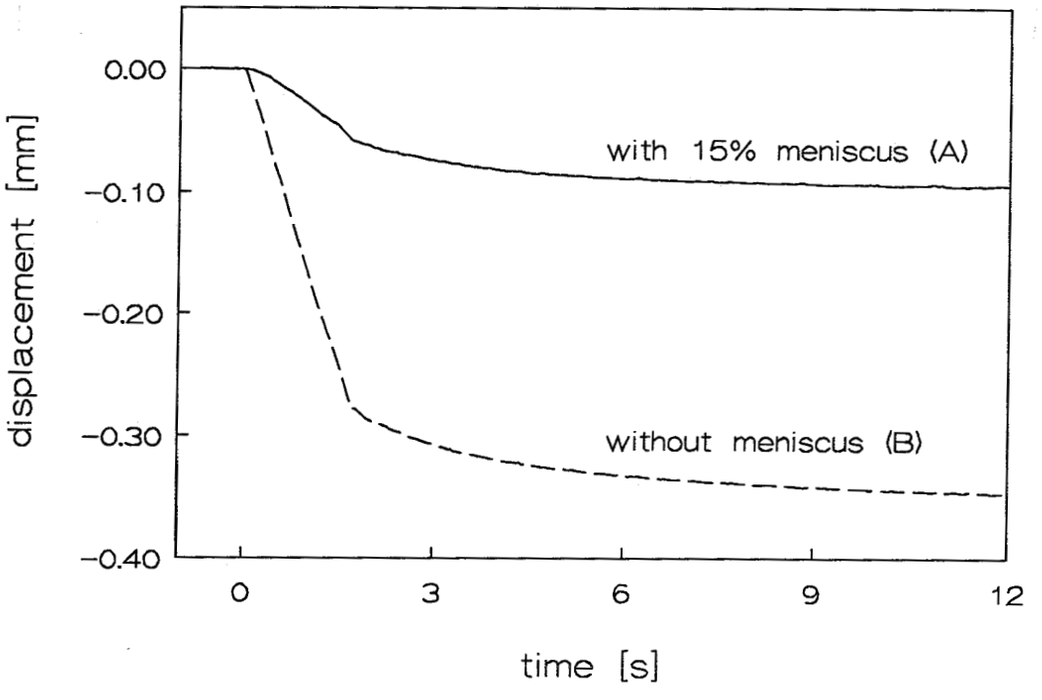

Figure 14: *V for model A and B.*

With the meniscus present between disc and indentor, part of the load will be carried by the indirect contact. As the load is distributed over a larger area, the indentation of the disc is reduced by a factor 3½. This directly results in a lower pressure P_1, which differs a factor 2½ at T_2. In course of time the difference becomes less.
For model B the pressure is concentrated around the middle of the disc, while with the

presence of the meniscus the pressure is more equally distributed over the cross section of the disc.

2.5.2 Parameterstudy

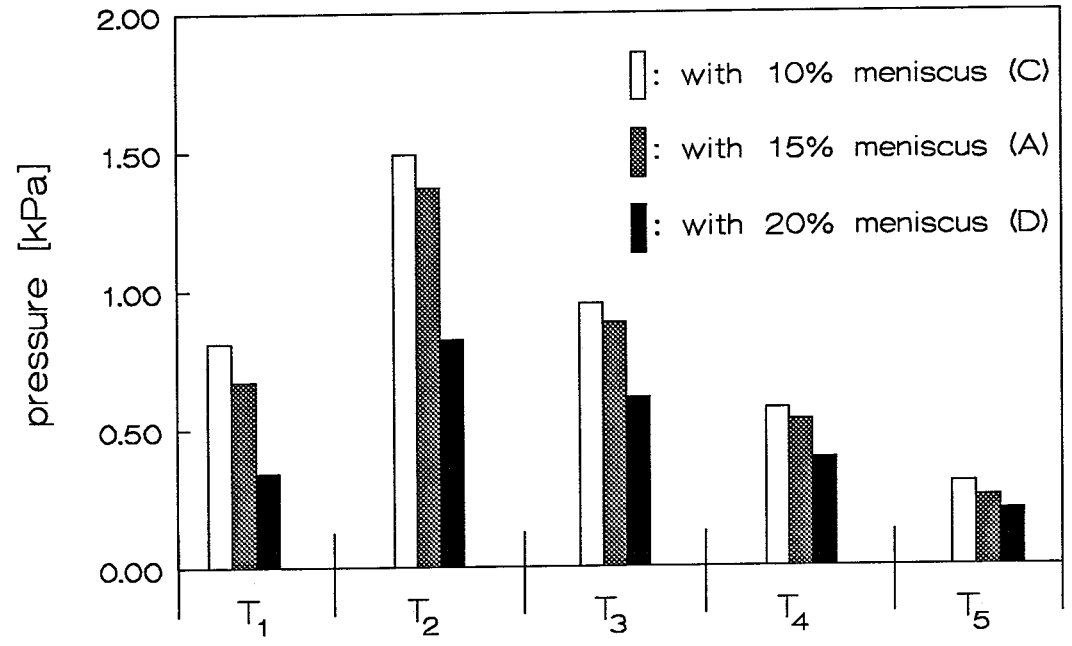

Figure 15: *P_1 for model A, C and D at five times.*

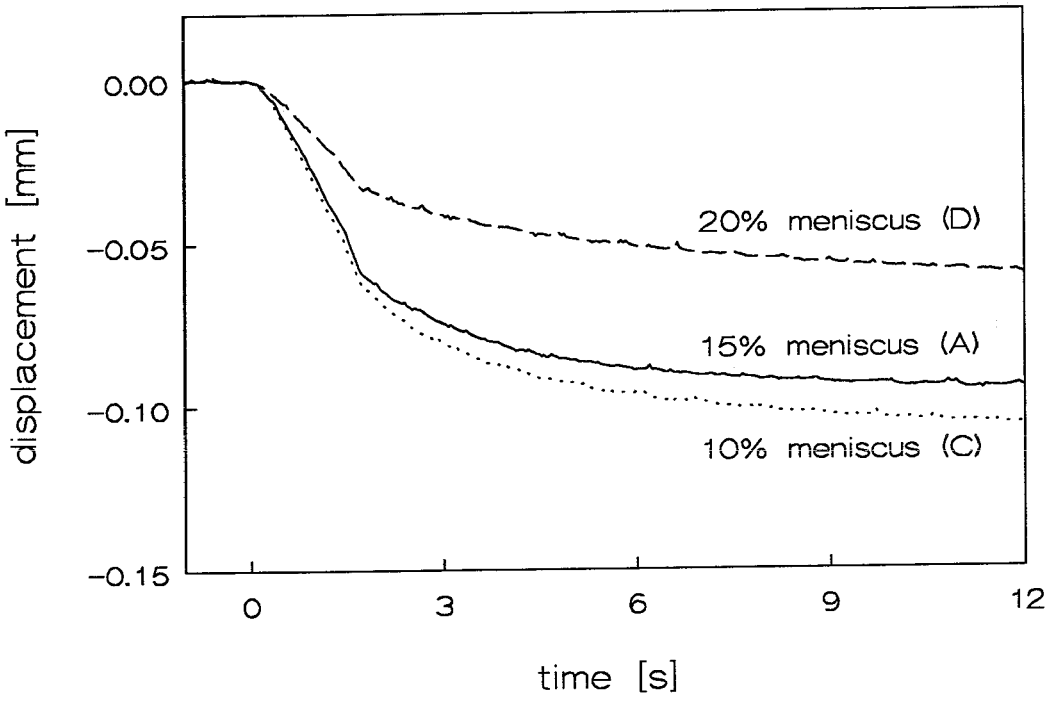

Figure 16: *V for model A, C and D.*

To investigate the influence of the material properties of the meniscus, a model with a 10% and a 20% meniscus have been tested. The 10% meniscus has a lower stiffness and higher permeability, for the 20% meniscus the opposite is true. It is expected that a lower stiffness of the meniscus will cause a larger indentation of the disc, causing an increase in pressure. On the other hand the fluid can easier flow out of the model due to a higher permeability of the meniscus and therefore a lower pressure can be expected.
Again at five times the pressures are compared, but now only for P_1. Figure 15 shows the resulting graph and in Figure 16 the displacement of the indentor for the different configurations can be seen. Model C (10%) gives a higher and model D (20%) a lower value at all times, both for P_1 and V. For the materials in this experiment the stiffness appears to have a larger influence on the pressure than the permeability.

2.5.3 Concluding Remarks

The experiments show reproducable results and therefore indicate the reliability of experimental set-up and procedures. With respect to the influence of the meniscus and its properties the following can be said. Via this indirect contact between disc and indentor the load is distributed over a larger area. This directly results in lower pressures, smaller indentation and a more equal distribution of the fluid pressure. The maximum pressure found in the middle of the disc is reduced by a factor 3½, the final displacement of the indentor by a factor 2½. For increasing stiffness of the meniscus, a decreasing indentation and lower fluid pressures are found. The effect of change in permeability appears to be small.

3. Numerical Analyses of a Knee Model

3.1 Model Description

For the numerical analyses the software package DIANA has been used. The finite element mesh of the model is given in Figure 17, together with the constraints. Isoparametric axisymmetric mixture elements are used for the meniscal ring and disc (Q8AXI), for the indentor truss elements (L4TRU*). A number of special elements, developed by Schreppers [1], are used to describe the contact between the different components. For a more detailed explanation of the numerical formulation of the mixtures is refered to Snijders [6].

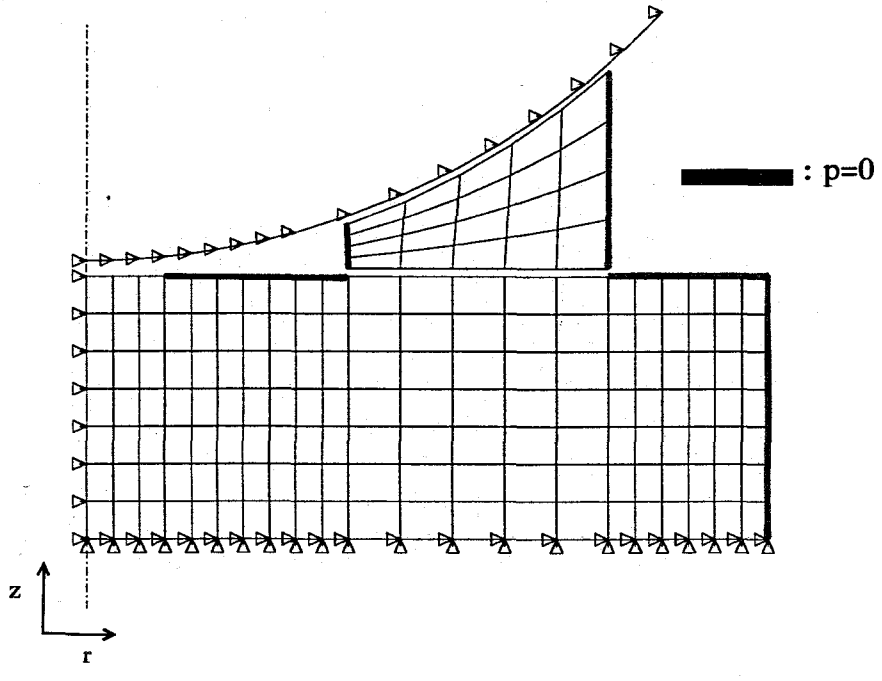

Figure 17: *FE-model of the knee contact together with the constraints (for sake of clearness the different components are shown without making contact, whereas in reality they touch).*

The lower end plane of the disc is fixed to a rigid impervious foundation, while the meniscal ring is allowed to slide frictionless along the surfaces of disc and indentor. The indentor is modelled as a rigid single phase material, whereas fluid flow between meniscus and disc is possible. At the outer surface of disc and meniscus pressure is assumed to be zero, as well as in the cavity enclosed by the three components.
Resembling the experiments the load was applied in two steps. After equilibrium was achieved for the preload, a second step of 1.5 N was applied to the indentor in 1.72 s. Beside parameters to describe the solid phase of the mixture elements (E,ν) the permeability K is required as input.

* Truss elements instead of axisymmetric elements are used for the indentor as only its vertical displacement is of interest. Furthermore the displacement can be seen as an extra set of constraints. The specially developed contact elements compensate for the discrepancy of dimension.

3.2 Modelling Strategy

As the materials are not fully characterized, the properties determined in the various experiments can only be used as estimations of the real values. To come around this problem the following strategy is applied: first calculations are made for a model without meniscus. The material properties from the indentation and permeability tests are used for a first approximation and are adjusted in accordance with results of model B, the experimental model without meniscus. Elastic modulus and permeability are varied until V(t=12s) and P_1(t=1.72s) are equal to those of model B. With these material properties a prediction is made for the experimental model with the 15% meniscus.
In Table 3 the different numerical models can be found with their material properties. Model E is the model with the material properties derived from material characterization, model F has the adjusted values. As can be seen the elastic modulus is changed about 60%, the permeability 75%. The same properties are used for the meniscus in model G, which gives a prediction for the model with the 15% meniscus.

Model	E [MPa]	K [mm^4/Ns]	Meniscus (Y/N)
E	0.25	85.	N
F	0.4	22.5	N
G	0.4	22.5	Y

Table 3: *Models with material properties, for all models v=0.38 [-].*

A parameterstudy is performed with respect to the material properties of the meniscus. As only the material properties of the 15% solution are adjusted in accordance with experimental results, the variety is more or less arbitrarilly chosen and can be found in Table 4. The meniscus in model H has a lower stiffness and higher permeabilty than the one of model G, for the meniscus in model I the opposite is true.

Model	E [MPa]	K [mm^4/Ns]
G	0.4	22.5
H	0.2	45.
I	0.8	12.25

Table 4: *Material properties of the meniscus (properties of the disc are same as in model F).*

Both in compression and indentation tests viscoelastic behaviour of the polyurethane was observed. The effect of this on the response of the model is not clear beforehand, as two time dependent processes interact with each other. Therefore also calculations are made with linear viscoelastic material models, which can be found in Table 5.

Model	E_0 [MPa]	E_1 [MPa]	λ_1 [s]	K [mm^4/Ns]	Meniscus (Y/N)
J	0.3	0.2	1.7	22.5	N
K	0.3	0.2	1.7	22.5	Y

Table 5: *Viscoelastic models with material properties for both disc and meniscus (present in model K).*

In the following paragraphs the results of the several numerical models are evaluated.

3.3 Results

3.3.1 Model with/without Meniscus

Figures 18 and 19 show the numerical results for model F and G, without and with meniscus respectively. For both models an increasing pressure is found during load application. This is not so obvious as it seems, as immediately when load application is initiated two contradictionary effects take place. The load is carried by the solid phase as well as by the fluid phase. When the load increases the pressure is expected to increase also. On the other hand the fluid can flow out of the model causing a decrease in pressure and the solid phase to carry a larger part of the load. In this case the first effect proves to have a larger influence.
After the load has been applied the pressure decreases due to the fluid flow out of the disc. The indentor displacement increases and more of the load is carried by the solid phase.
The highest pressure is much lower for the model with meniscus. The meniscus' presence also gives a totally different pressure distribution and indentation. For both models the highest pressure is found in the middle of the disc, but going outward a more equally distribution is found for the model with meniscus. Moreover P_4 and P_3(at T_1 and T_2) give higher pressure for the model with meniscus. The indentation of the disc is much lower for the model with meniscus.

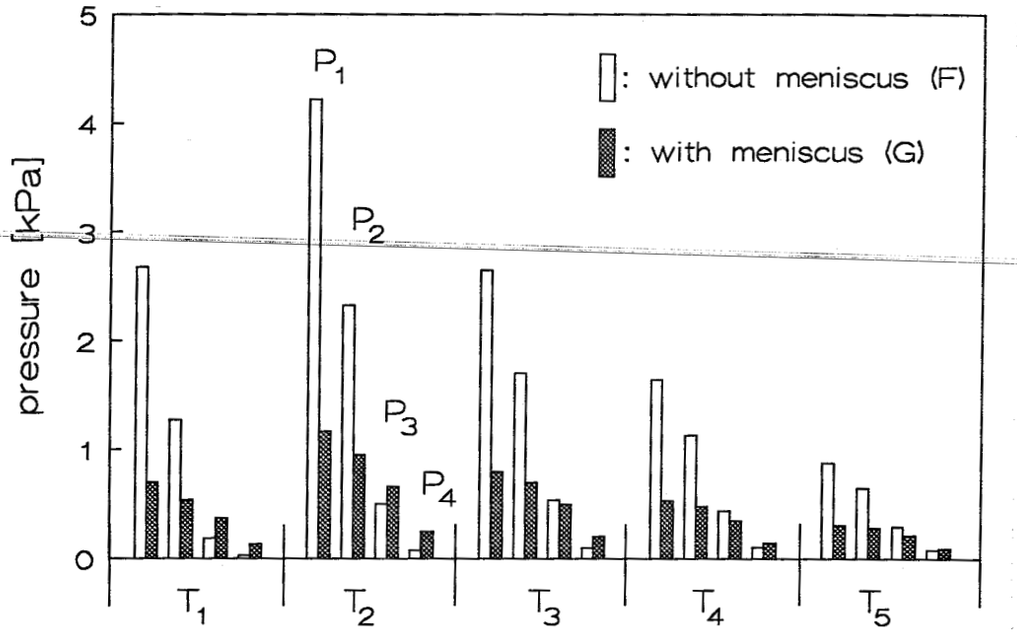

Figure 18: *P_1 to P_4 for model F and G at five times.*

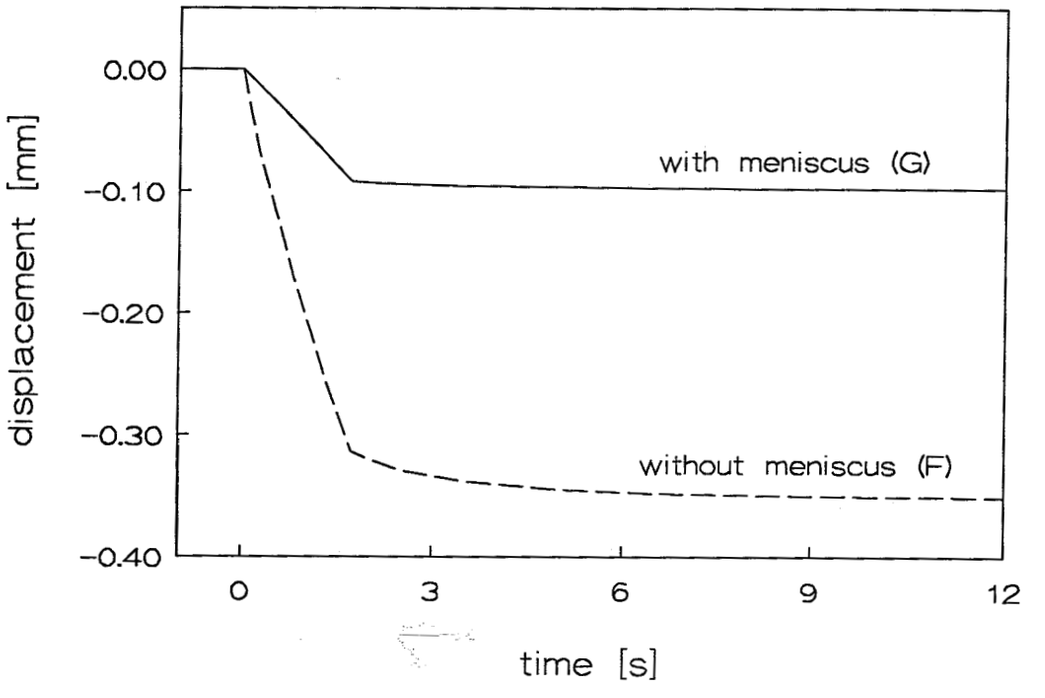

Figure 19: *V for model F and G.*

3.3.2 Parameterstudy

Figures 20 and 21 show the results for the models with different material properties for the meniscus. Although the variation of the parameters is more or less arbritrarilly chosen, the same characteristics are found as in the experiments. As both stiffness and permeability are changed by a factor 2, the change in stiffness appears to have a larger influence: for increasing stiffness (model I) a decrease in magnitude of V and P_1 is found.

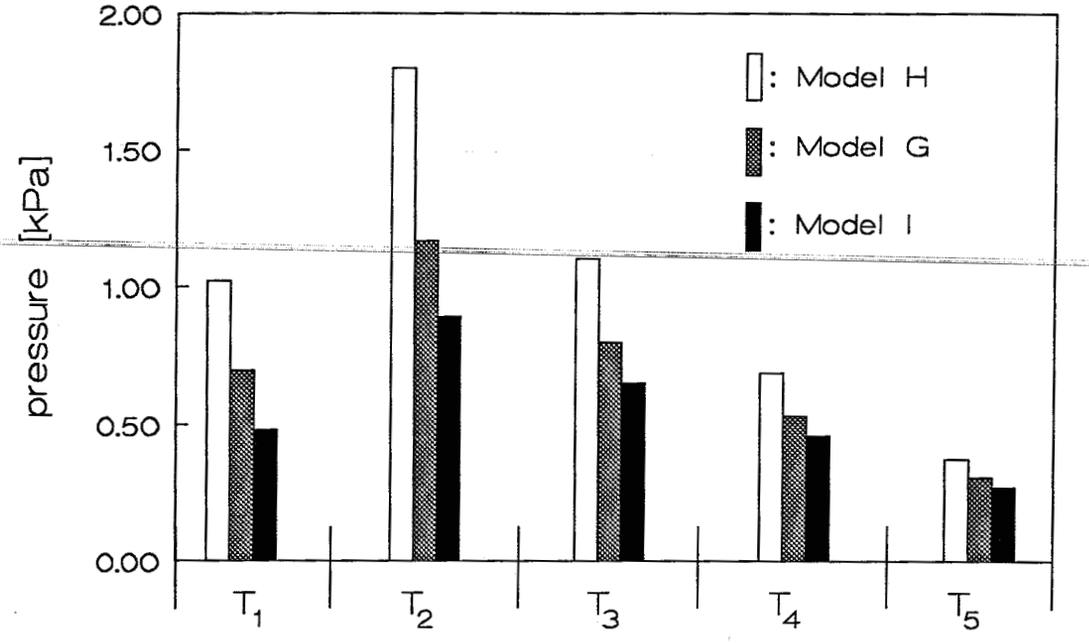

Figure 20: *P_1 for model G, H and I at five times. Model H having a lower stiffness and higher permeability than model G. For model I the opposite is true.*

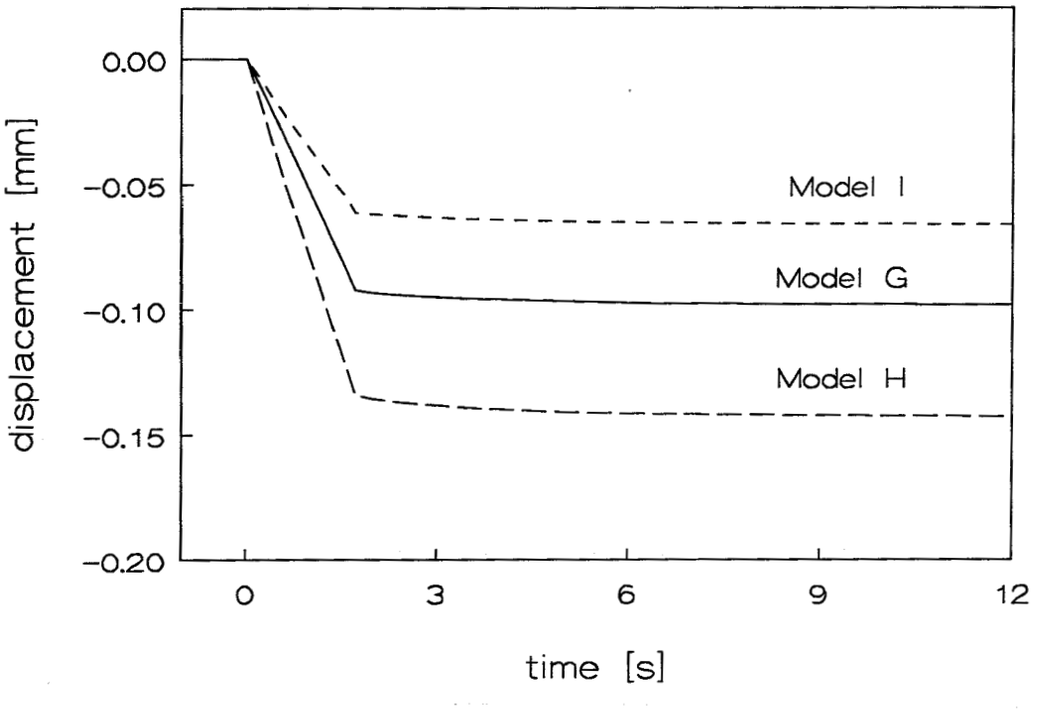

Figure 21: *V for model G, H and I. Model H having a lower stiffness and higher permeability than model G. For model I the opposite is true.*

3.3.3 Effect of Viscoelastic Behaviour

Figure 22 and 23 show the results of the models without meniscus, model F with a linear elastic and model J with a viscoelastic material behaviour to describe the solid matrix of the disc. With the viscoelastic material behaviour an extra relaxation time is introduced.

After the load is applied, the displacement of the indentor not only increases because of fluid flow out of the disc, but also due to the creep behaviour of the solid constituent. This last effect causes the fluid to carry a larger part of the load and so the pressure to drop at a slower rate in course of time. Even when the pressure becomes zero, no equilibrium has been achieved for the solid phase and the indentation still increases.
The same characteristics are found for the models with meniscus (which are not shown here).

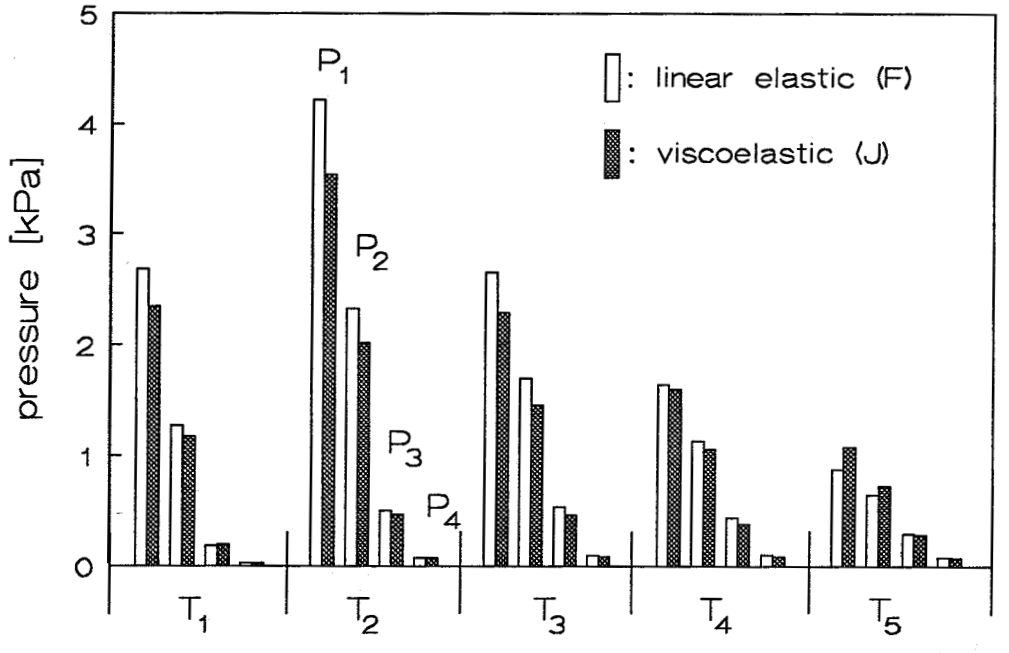

Figure 22: *P_1 to P_4 for model F and J at five times.*

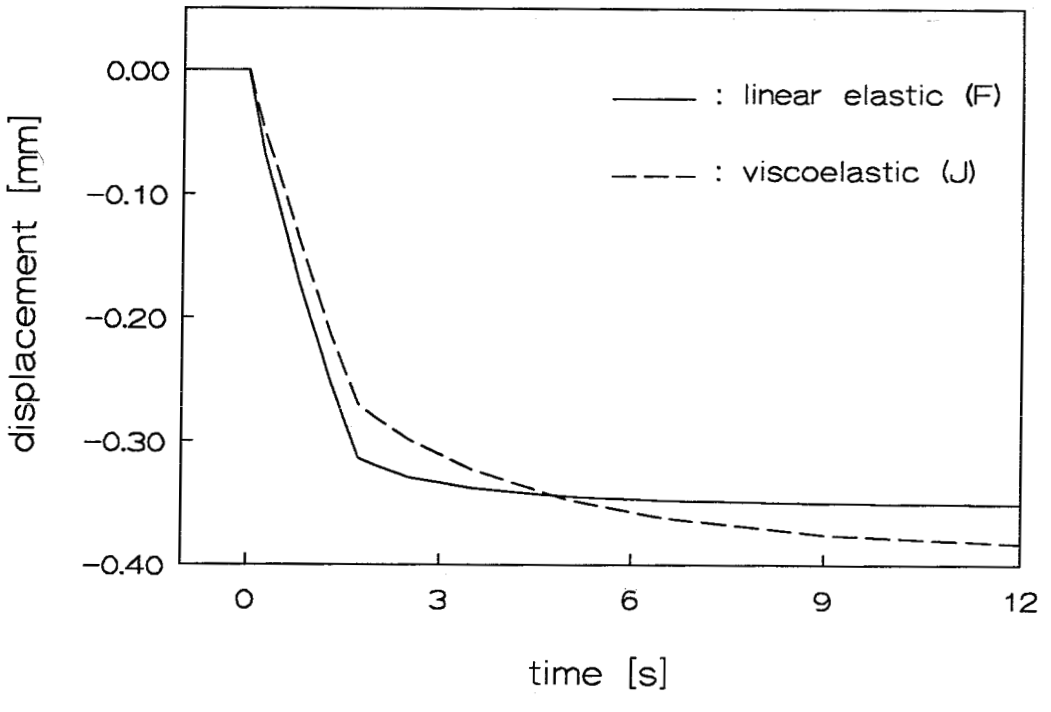

Figure 23: *V for model F and J.*

3.3.4 Concluding Remarks

In the numerical analyses the influence of the meniscus and its material properties are investigated. Also the effect of viscoelastic behaviour of the solid constituent is examined. With the meniscus present between indentor and disc, the indentation and the pressure in the middle of the disc become much lower. The pressure distribution over the cross section of the disc is more smoothly.
In the parameter study both stiffness and permeability of the meniscus were changed by a factor 2. The change in stiffness appears to have a larger influence on the pressure than the change in permeability. For increasing stiffness a decrease in magnitude of the pressure in the middle of the disc and the displacement of the indentor is found.
Creep behaviour of the solid constituent causes the pressure to drop at a slower rate after load application and the indentation to progress slowly even when the fluid phase does not contribute to the load bearing.

Comparing these remarks with the ones resulting from the experiments, already a qualitative agreement is found with respect to the presence of the meniscus and the parameter study. A confrontation of the numerical with the experimental results and a quantitative comparison is made in the next chapter.

4. Confrontation Numerical/Experimental Results

In this chapter the numerical results will be compared to the experiments. The results of the numerical model without meniscus are fitted on the experiments only at two points. First a quantitative comparison will be made for this model with respect to the pressure distribution and the indentation for the entire duration of the experiment. For the models with meniscus only a quantitative comparison can be made for the model with a 15% meniscus, as for the 10% and 20% materials the parameters were not determined. At the end of this chapter the results of the viscoelastic model with meniscus are compared to the experiments.

4.1 Model without Meniscus

When the pressures resulting from the numerical elastic model (F) are confronted with the experiments (model B) in Figure 24 a fairly good resemblance is found at T_1 and T_2. P_1 shows the best agreement, which is not surprising as this parameter is fitted on the experiments at T_2. Going from the middle of the disc outward, we see at T_2 that P_2 differs about 16% and P_3 40% from the experiment. P_4 in the numerical model is positive, but the negative value in the experiment probably can be ascribed to bending of the disc during loading. As the lower end plane is held down to the underground due to adhesion a negative pressure results at the outer edge of the disc.
After load appliance, T_2 to T_5, a faster decrease of the pressures is found in the experiment. Also the pressure is more equally distributed over the surface of the disc.
Figure 25 shows the displacement of the indentor for the two models. In the numerical model the indentor reaches its final displacement only a few seconds after the load has been applied, in the physical model the displacement progresses slowly and is still increasing at the end of the experiment.

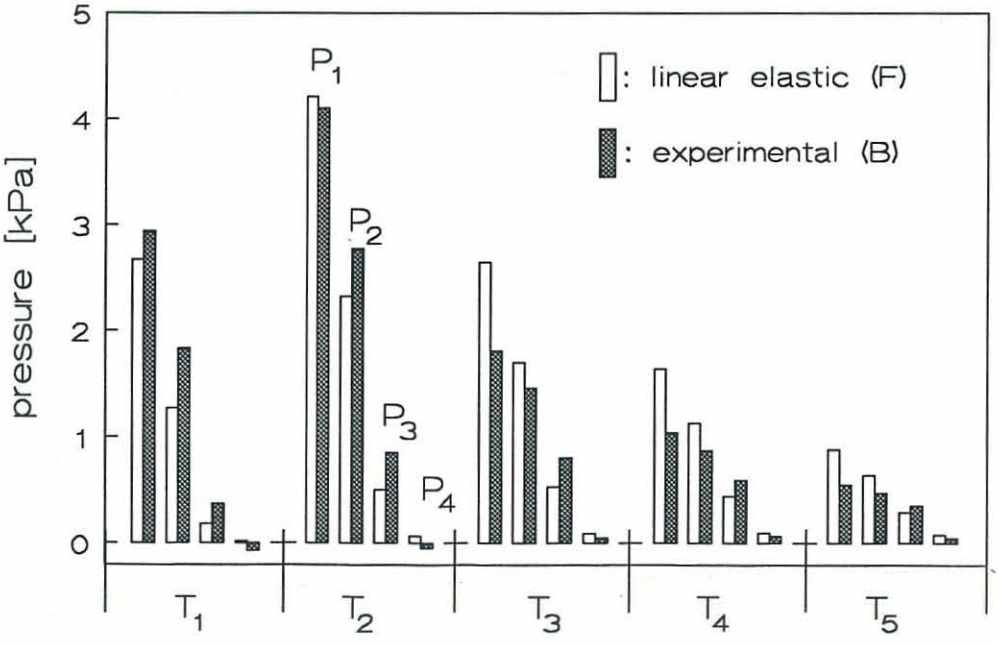

Figure 24: *P_1 to P_4 for model F and B at five times.*

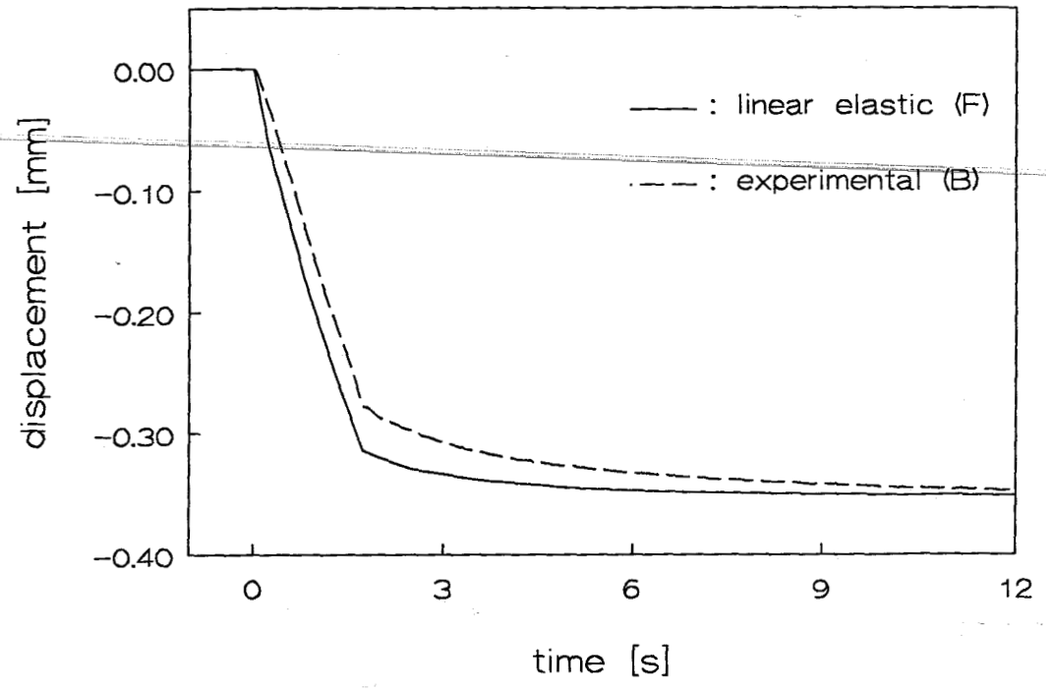

Figure 25: *V for model F and B.*

4.2 Model with Meniscus

4.2.1 Linear Elastic

The first two points where a comparison should be made for the models with meniscus are $P_1(t=T_2)$ and V(t=12s), as the model without meniscus is fitted on these points. Doing so, immediately striking quantitative agreements are found between the numerical model (G) and experimental model (A); P_1 differs only 15% and V 5% (Figures 26 and 27).
Moreover the differences for P_2 and P_3 are also approximately 15% and even at the other moments the numerical results resemble the experimental ones. For P_4 however a relatively poor agreement is found.
Some of the differences encountered for the models without meniscus (4.1) also hold here. For T_2 to T_5 the pressures in the experiments decrease faster. The discrepancy for the displacement of the indentor is now even more. Whereas in the numerical model the indentor reaches its final displacement almost immediately after load application, in the experiment the indentation progresses slowly (even at the end of the experiment).
Whether this effect can be ascribed to viscoelastic behaviour of the solid constituent will be examined in the next section.

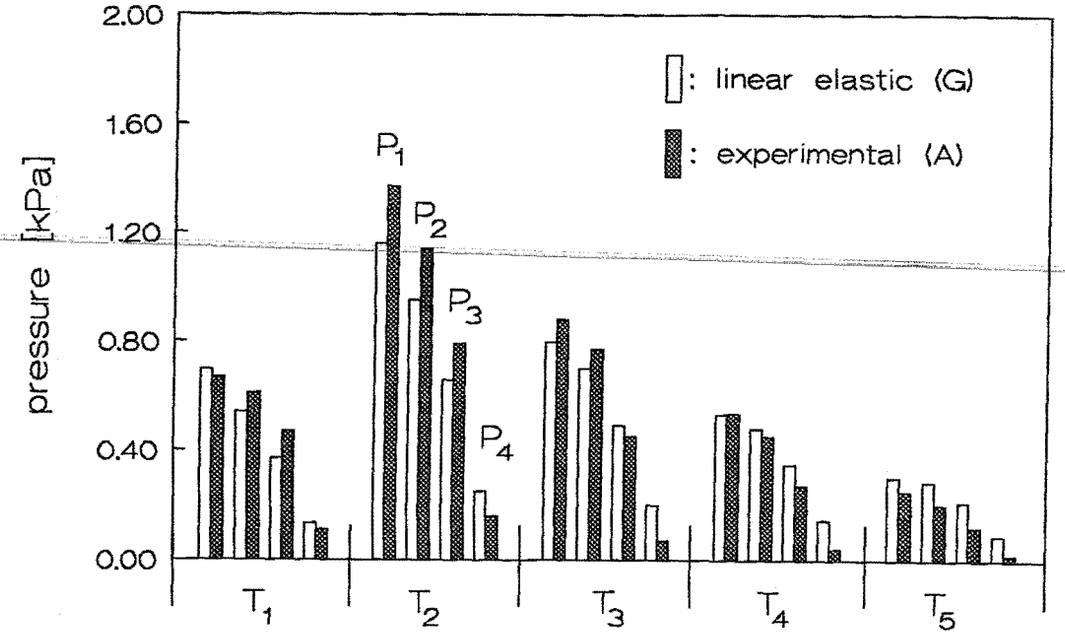

Figure 26: *P_1 to P_4 for model A and G at five times.*

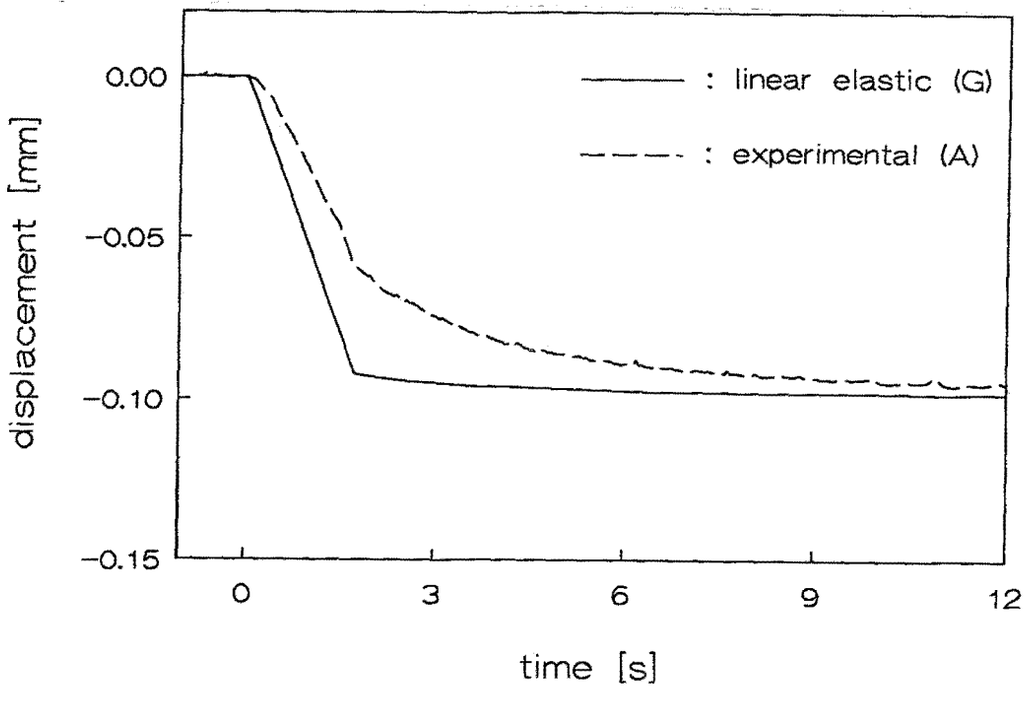

Figure 27: *V for model A and G.*

4.2.2 Viscoelastic Behaviour

With the description of the solid phase by a 3-parameter Maxwell chain model (model K), a better resemblance is found for displacement of the indentor (Figure 29). After the load has been applied the numerical results only differ a constant factor from experiment.
However, compared to the linear elastic model, the introduction of viscoelastic behaviour causes the pressures to drop at even a slower rate after load application. Thus the

differences at later moments to become larger.
When the viscoelastic behaviour of the solid phase would be described by a 5-parameter instead of the 3-parameter Maxwell model, even a better agreement is expected. The 3-parameter model generally gives a good description for the first response after load application and at the end of the experiment. With a 5-parameter model a better description can be achieved for the complete duration of the compression test and thus for the indentation experiments. The model contains an extra damping factor causing the displacement of the indentor to increase at a slower rate. Both de Heus [4] and Goijaerts [5] described the material behaviour of the polyurethane with a 5-parameter model.

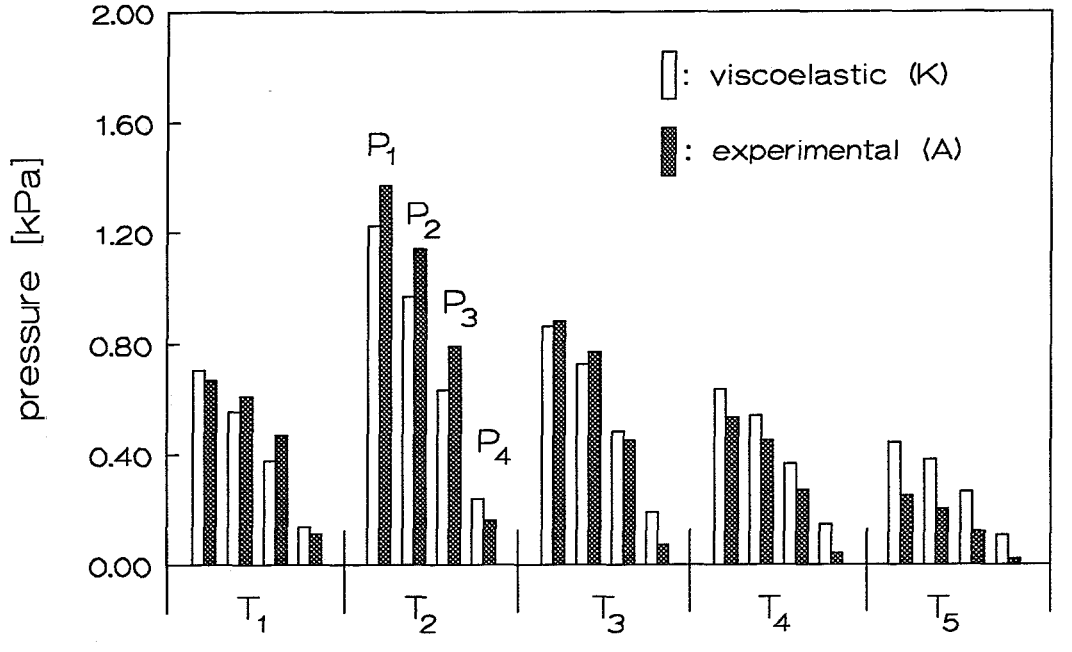

Figure 28: *P_1 to P_4 for model K and A at five times.*

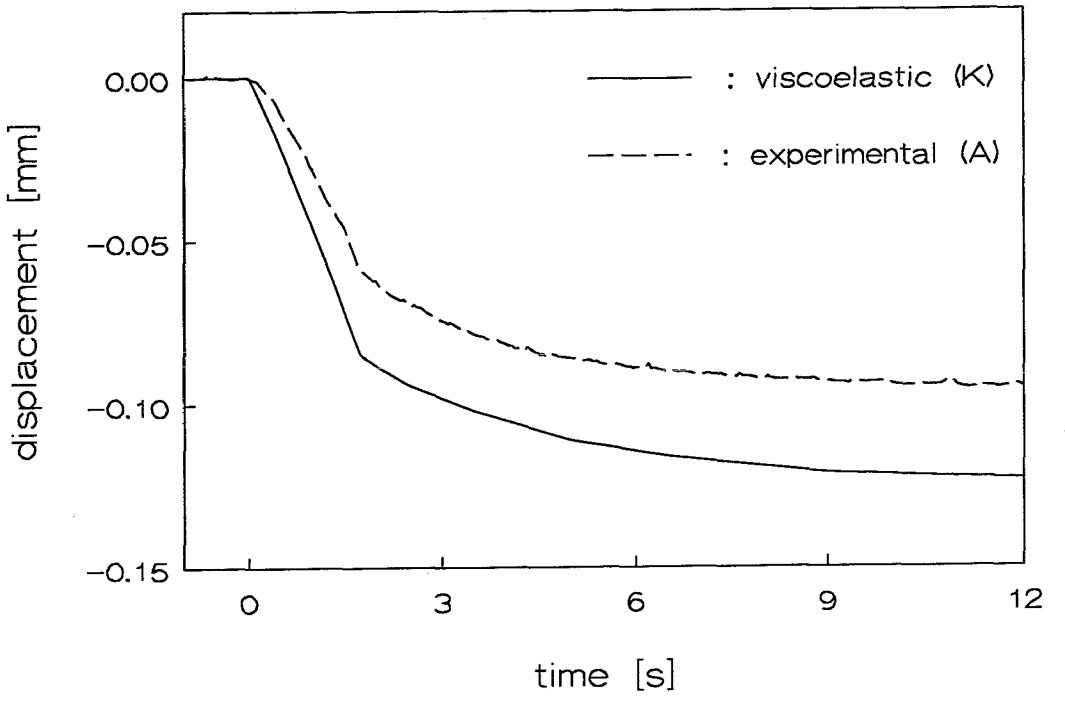

Figure 29: *V for model K and A.*

4.3 Concluding Remarks

Comparing the results of the numerical analyses with experiments striking resemblances, but also some differences, are found.

Although the numerical model without meniscus is fitted on the experiment, the agreement between the pressures becomes poorer towards the edge of the disc and a more equal distribution of the pressures is found in the experiment.

For the linear elastic model with meniscus the highest pressures of P_1 to P_3 differ only 15% and the final displacement 5%. The indentation as a function of time, however, completely differs from the experiment. The viscoelastic model shows a better agreement for the indentation: after load appliance it only differs a constant factor. With the description of the solid phase by a 5-parameter Maxwell model a good resemblance for the indentation is expected for the entire duration of the experiment.

For both linear elastic models a slower decrease of magnitude of the pressure is found after load appliance. In the viscoelastic models this effect even becomes larger.

5. Discussion, Conclusions and Recommendations

5.1 Discussion

Experiments as well as numerical analyses have been performed on a model of the knee contact. A total of four configurations are tested, which differ from each other with respect to the meniscus' presence and its material properties.

In the experiments the response of the model is found to change considerable with a meniscal ring present between indentor and disc. The maximum measured pressure is reduced by a factor 2½ and the final displacement of the indentor by a factor 3½. The pressure also shows a more equal distribution over the cross section of the disc. With a parameter study decreasing indentations and pressures are found for increasing stiffness of the meniscus, while the effect of change in permeability appears to be small. Viscoelastic behaviour is observed for the solid constituent of the mixtures.
The first numerical analyses are performed with a linear elastic material behaviour and qualitatively the same results are found as in the experiments. Describing the solid phase with a 3-parameter Maxwell chain model shows that creep behaviour causes the indentation to progress, and the pressure to drop, at a slower rate after load appliance.
Confronting the numerical results with the experiments striking resemblances are found both for the model without and with meniscus. The maximum values of P_1 to P_3 show a fairly good agreement with the experiments. A relitatively poor agreement however is found for P_4.
For the linear elastic model with meniscus the final indentation of the disc differs only 5% from experiment, but the displacement of the indentor differs as a function of time. A better resemblance for the displacement is found for the entire time interval by describing the solid matrix with a 3-parameter Maxwell chain model.

The experiments showed reproducable results and therefore indicate the reliability of experimental set-up and procedures. The resemblances between experiments and numerical analyses suggest the validaty of the numerical formulation.

Also some differences are found and the possible discrepancies between experiments and numerical analyses should be investigated in order to locate the causes.
The largest influence is expected to come from the description of the material behaviour of disc and meniscus:

- Firstly, as already is mentioned, a 3-parameter Maxwell chain model used to describe the material behaviour of the solid matrix gives a better resemblance for the indentation than the linear elastic analyses. It is recommended to fit a 5-parameter model for the polyurethane, as this also has been shown by de Heus and Goijaerts to describe the material behaviour better. The fit however should be done at the same disc as used in experiments, as the fabrication proces is not fully

controlable and reproducable.

- Secondly, it is likely that with the present fabrication proces the materials may contain some inhomogeneity and anisotropy. At the upper and lower surface of the disc smaller holes, and therefore lower permeability, can be expected than in the middle due to different cooling rates. As in the numerical analyses the disc is modelled homogeneous and isotropic, this could account for the different relaxation times between numerical models and experiments and for the different pressure distribution for the model without meniscus. To check wether inhomogeneity causes the differences, the disc could numerically be modelled consisting of three layers. The upper and lower layer should be modelled with a lower permeability and/or higher stiffness than the middle one.

Further there are some assumptions in the numerical analyses with respect to the geometry of disc and meniscus and their constraints:

- The outer edge of the physical disc might be slightly lifted from the underground or might be thinner than the rest of the disc. The fluid could flow freely out of the lower surface of the disc there. This should cause a faster drop of the pressure going outward, and can be a possible explanation for the poor agreement found for P_4.
- Some other assumptions which are not yet looked into are the frictionless sliding of meniscus and the fixation of the lower end plane of the disc in radial direction. These could be verified by measuring several displacements at the outer edge of meniscus and disc in the experiments or with numerical simulations to judge the effect.

And as last a remark about the FE-modelling:

- As in the numerical formulations discretization occurs both in time and place, the influence of a finer mesh and smaller time steps can be investigated.

5.2 Conclusions and Recommendations

The experiments and numerical analyses performed in this study show qualitative as well as quantitative agreements. Also some differences are found but these probably can be ascribed to the more complex physical material behaviour of disc and meniscus. Therefore the results of this study indicate the validity of the numerical modelling.

Further evaluation of the experiments also for the higher and lower load step is interesting as this can show more of the effect of load bearing by solid and fluid phase during load application.

Viscoelasticity of the solid constituent of the mixture components appears to have a large influence on the response of the model. A better agreement for the indentation is expected with the description of the material behaviour of the polyurethane by a 5-parameter Maxwell chain model.

The experimental set-up has proved to be reliable. For future experiments the measurement of the displacement of the meniscus however will show more about the

contact conditions (slip or stick) between meniscus and indentor or disc. To achieve better resemblances both for pressures and indentation for the entire duration of the experiment one can try to adjust the present fabrication method of disc and meniscus or look for another (linear elastic, homogeneous, isotropic) solid constituent.

References

[1] Schreppers, G.J.
Force transmission in the tibio-femoral contact complex
Ph.D.-thesis Eindhoven University of Technology, juni 1992

[2] Oomens, C.W.J.
A mixture appraoch to the mechanics of skin and subcutis
Ph.D.-thesis Twente University of Technology, juni 1985

[3] Feron, R.P.M.J.
Ontwerp van een meetopstelling ter validatie van een numeriek kniemodel
Eindhoven University of Technology, internal report W.F.W.92.114, 1992

[4] Heus, H.J. de
Model materials for validation of mathematical models describing biological tissue behavior, in: Computer Methods in Biomechanics & Biomedical Engineering,
Edited by: J. Middleton et al., Books and Journals Int. LTD, 1992, p. 210-219

[5] Goijaerts, A.
Materiaalgedrag van PUR-schuim©
Eindhoven University of Technology, internal report W.F.W.93.082, 1993

[6] Snijders, H.
The Triphasic Mechanics of the Intervertebral Disc: A theoratical, numerical and experimental analysis
to be published, 1993

[7] Gonzalez, R.C. , Wintz, P.
Digital image processing
Addison-Wesley Publishing Company, 1977

[8] Deurhof, M.
Contactloze positie-meting van markeringen met een diameter van 10 tot 100 µm
Eindhoven University of Technology, internal report W.F.W.92.070, 1992

[9] Vercammen, R.
Ontwikkeling van een meetprocedure voor permeabiliteitsmetingen
Eindhoven University of Technology, internal report W.F.W.91.013, 1991

Appendix A

Resultaten Metingen

In deze bijlage zijn alle meetresultaten opgenomen voor de verschillende modellen (Tabel A1). Elk model is op drie niveaus belast: F=0.75, 1.5 en 2.25 N. Om het geheel wat overzichtelijker te maken zijn de resultaten per model op één bladzijde gezet. Sommige drukmetingen vertonen plotselinge pieken in het verloop, wat te wijten is aan verschuiven van het laadbakje tijdens het aanbrengen van de belasting. Opmerkelijk is nog dat de drukken voor de middelste belasting (F=1.5 N) veel hoger zijn dan voor de laagste (F=0.75 N). Het verschil tussen de hoogste en de middelste belasting daarentegen is veel kleiner en de drukken vertonen een vlakker verloop. Dit duidt erop dat de druk voor de hoogste belasting sneller daalt door uitstromen van de vloeistof, dan dat de druk stijgt als gevolg van de toenemende belasting.

Model	A	B	C	D
materiaal meniscus	15%	--	10%	20%

Tabel A1: *Modellen met hun variatie in meniscus (in alle modellen was de schijf gemaakt van een 15% oplossing en 10mm hoog)*

Model A (met 15% meniscus)

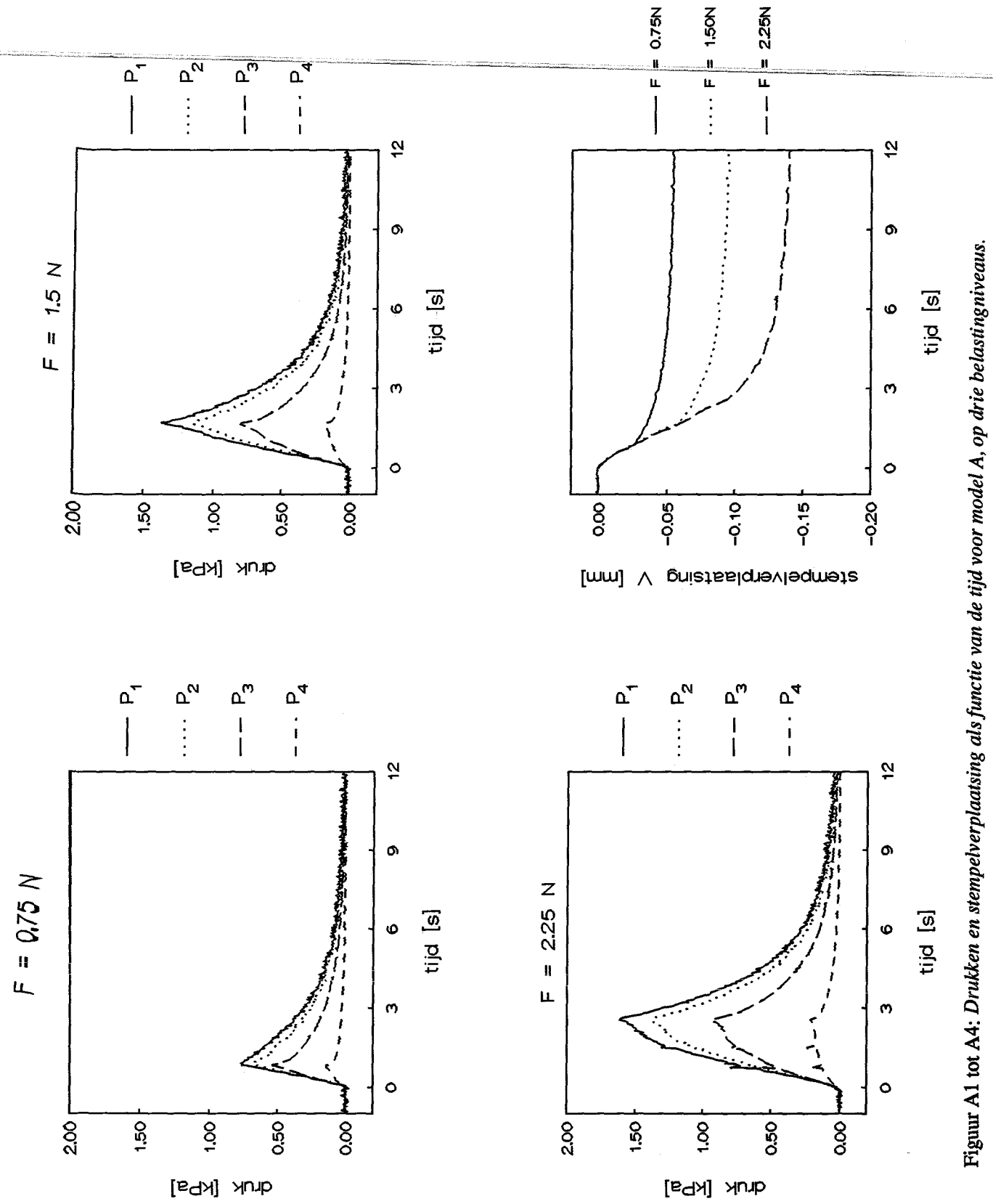

Figuur A1 tot A4: *Drukken en stempelverplaatsing als functie van de tijd voor model A, op drie belastingniveaus.*

Model B (zonder meniscus)

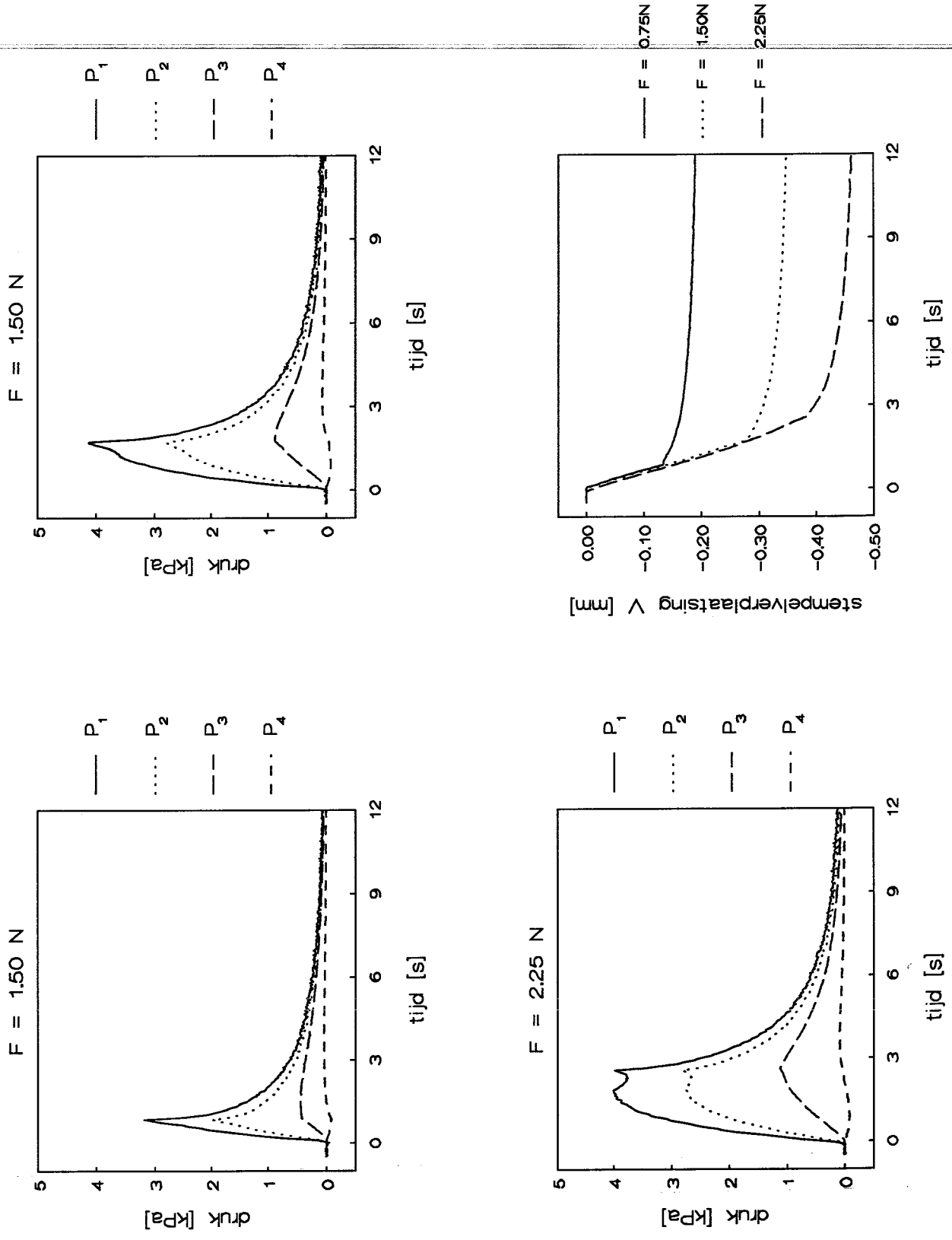

Figuur A5 tot A8: ***Drukken en stempelverplaatsing als functie van de tijd voor model B, op drie belastingniveaus.***

Model C (met 10% meniscus)

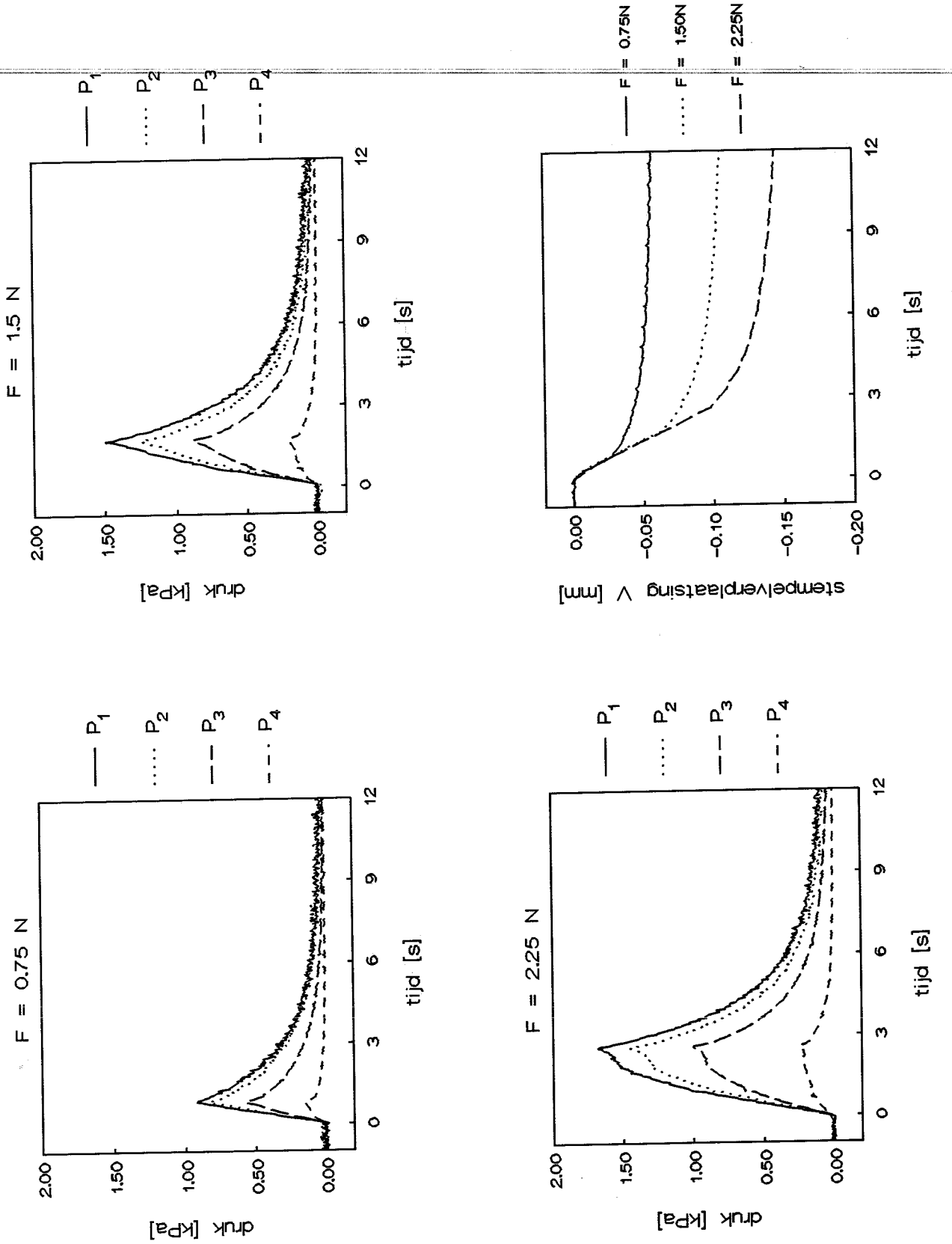

Figuur A9 tot A12: *Drukken en stempelverplaatsing als functie van de tijd voor model C, op drie belastingniveaus.*

Model D (met 20% meniscus)

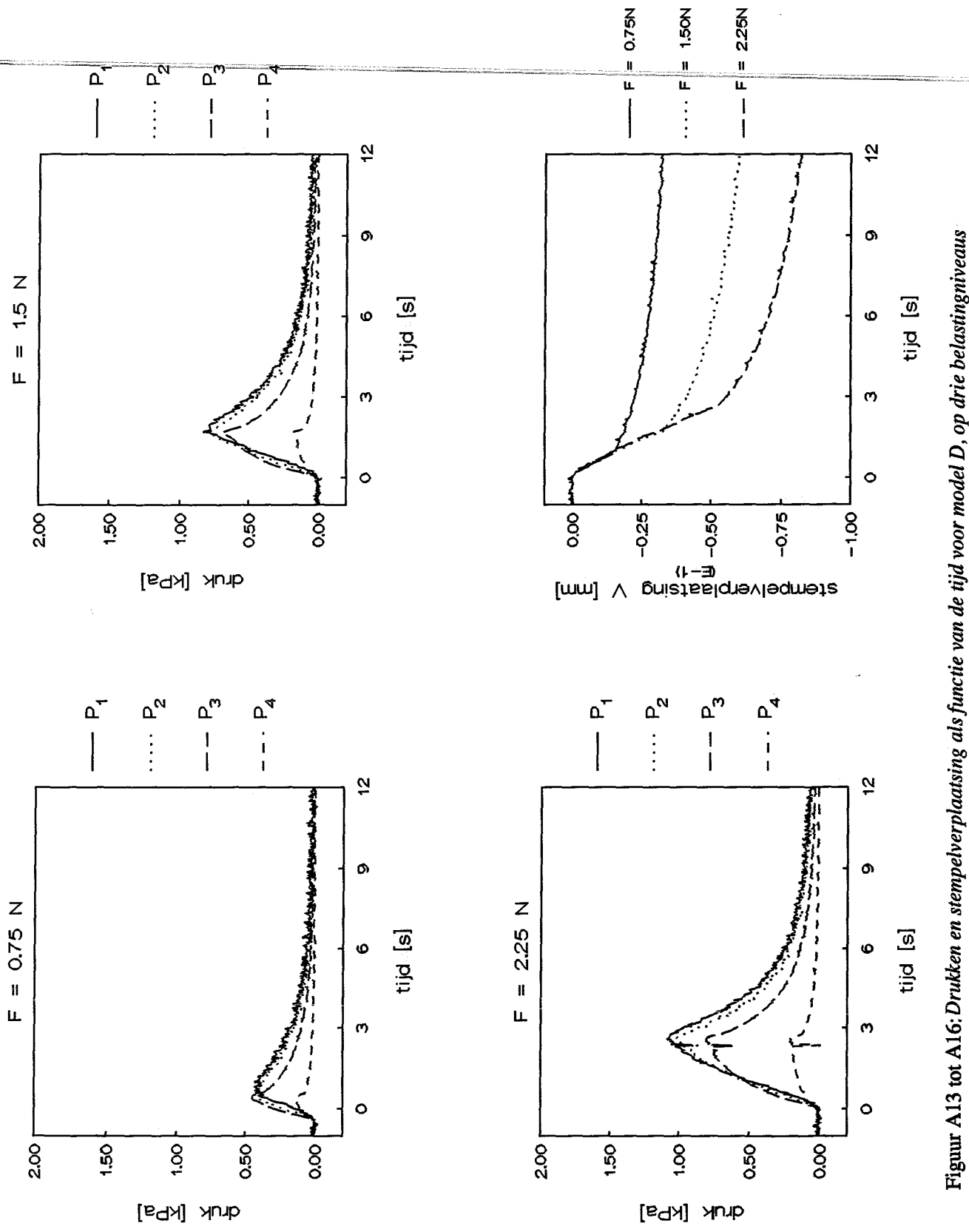

Figuur A13 tot A16: *Drukken en stempelverplaatsing als functie van de tijd voor model D, op drie belastingniveaus*

Appendix B

Verplaatsing Meniscus

De eerste opzet was om ook de verplaatsing van de buitenrand van de meniscus te meten en te vergelijken met numerieke berekeningen. De gevolgde procedures, verwachte meetnauwkeurigheid en resultaten zullen worden beschreven in deze bijlage. Uit de resultaten blijkt het meetconcept niet te voldoen en zullen aanbevelingen gedaan worden voor eventuele opvolger(s).
Aangezien de verplaatsingen van de meniscus klein zijn en er niet van dichtbij gemeten kan worden, is gebruik gemaakt van een lange afstands microscoop. Deze staat buiten het bakje waarin het model zich bevindt en is met een X-Y tafel aan het frame bevestigd. Hij wordt scherpgesteld op de platte kop van een speld die, halverwege de buitenrand, ca. 3mm in de meniscus is gestoken (zie Figuur B2). De andere kant van de speld wordt belicht zodat een gaatje (∅=0.1mm), aanwezig in de kop, goed zichtbaar wordt. Achteraan de microscoop bevindt zich een camera, zodat de beweging van het gaatje opgenomen kan worden op een videoband. Tevens is een digitale klok in het videobeeld gemixt om de beelden te koppelen aan de andere meetsignalen. Later wordt met het beeldbewerkings-programma TIM het middelpunt van het gaatje bepaald op verschillende tijdstippen. De verplaatsing is dan bekend in aantal beeldpixels en dient nog omgerekend te worden naar millimeters. Hieronder volgt een beschrijving van de instelprocedure en de nauwkeurigheid waarmee gemeten wordt.

B.1 Instelprocedure en Nauwkeurigheid

De nauwkeurigheid is naast externe invloeden afhankelijk van de volgende procedures die elk afzonderlijk besproken zullen worden:

- uitlijnen van de microscoop
- bepalen middelpunt met TIM
- calibratie van de beeldgrootte

De maximale absolute fout is bij elk onderdeel aangegeven met f.

B.1.1 Uitlijnen Microscoop

Het assenstelsel van de microscoop dient zo goed mogelijk overeen te komen met die van het model. De afwijkingen van de assenstelsels kunnen uitgedrukt worden in hoekverdraaingen om de verschillende assen; hier aangeduid met α, β en γ voor resp. de x, y en z-as (zie figuur B1).

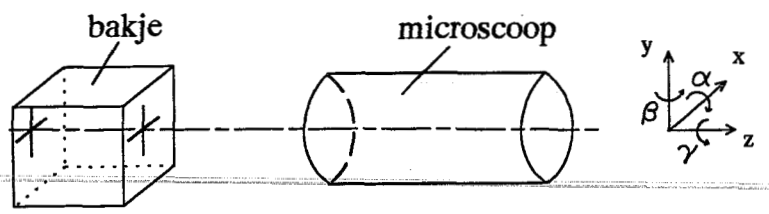

Figuur B1: *uitlijnen microscoop en definitie assen en hoekverdraaïngen*

De optische as van de microscoop wordt in de lijn van 2 kruizen, aangebracht aan weerzijden van het bakje, gezet. Daarna is de microscoop langs 1 van de kruizen bewogen om ook x en y-as uit te lijnen. De hoekverdraaïngen die bij dit uitlijnen kunnen voorkomen zijn afgeschat en in Tabel B1 gezet tezamen met de fout in de verplaatsingsmeting die ze tot gevolg hebben. Een hoekverdraaïng om de x-as geeft alleen een procentuele fout in de verticale verplaatsing, om de y-as alleen in de horizontale verplaatsing. Een hoekverdraaïng om de z-as geeft in beide verplaatsingen een afwijking die afhankelijk is van hoek φ (φ aangegeven in Figuur B2). In Tabel B2 is voor drie verschillende hoeken φ de afwijking berekend. Zoals uit de tabellen te concluderen is, is de verplaatsingsbepaling het gevoeligst voor een hoekverdraaïng γ.

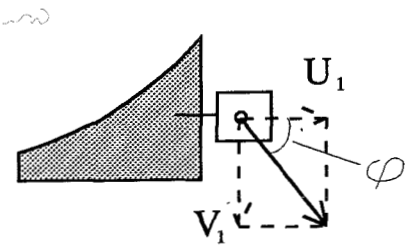

Figuur B2: *definitie hoek* φ

hoek	maximale verdraaïng [°]	ΔU_1 [%]	ΔV_1 [%]
α	0.6	-	0.006
β	4.0	0.25	-
γ	1.0	1.7*tanφ	1.7/tanφ

Tabel B1: *maximale hoekverdraaïngen met de veroorzaakte fout*

φ [°]	ΔU_1 [%]	ΔV_1 [%]
10	0.3	10.0
45	1.7	1.7
80	10.0	0.3

Tabel B2: *procentuele afwijkingen t.g.v. hoekverdraaïng* γ *voor verschillende hoeken* φ *bepaald*

De totale fouten ten gevolge van het uitlijnen van de microscoop in x- en y-richting zijn:

$$f_{ux} = (0.0025 + 0.017*\tan\varphi) * U_1$$

$$f_{uy} = (0.00006 + 0.017/\tan\varphi) * V_1$$

B.1.2 Bepalen Middelpunt met TIM

Met het programma TIM wordt op een later tijdstip een videobeeld ingelezen en bewerkt. Het beeld wordt onderverdeeld in alleen zwarte en witte pixels, het gaatje (=witte pixels) wordt geselecteerd en hiervan het zwaartepunt bepaald. Om de nauwkeurigheid van deze procedure te weten is 1 beeld 20 maal bewerkt en hiervan de 95% betrouwbaarheids intervallen bepaald (uitgaande van normale verdeling). Aan het einde van deze appendix staat het TIM programma zpunt.cmd dat gebruikt is voor de bepaling van het zwaartepunt.

f_{tx} = 0.11 pixels
f_{ty} = 0.08 pixels

B.1.3 Calibratie Beeldgrootte

Met TIM wordt dus de beweging van het zwaartepunt van het gaatje bepaald in pixels. Deze moet nu nog gekoppeld worden aan verplaatsingen. Daartoe wordt de beeldgrootte bepaald met behulp van twee verplaatsingsopnemers die aan de X-Y tafel bevestigd zijn. Voordat een meetsessie plaatsvond is eerst in elk hoekpunt van het camerabeeld het zwaartepunt van het gaatje bepaald en gerelateerd aan de uitlezing van de verplaatsingsopnemers, zoals te zien is in Figuur B4.

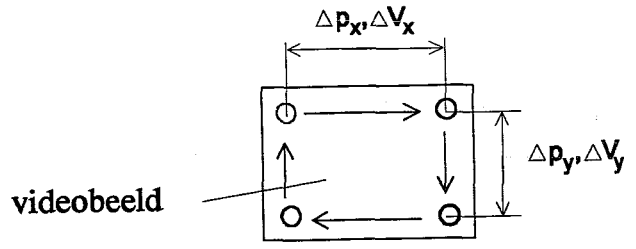

Figuur B4: *bepaling beeldgrootte*

Het spanningsverschil van de opnemers kan direct omgezet worden in een verplaatsing (zie calibratie curves bijlage D). De onnauwkeurigheid van de verplaatsingsopnemers werken hierbij door op de nauwkeurigheid van de bepaling van de pixelafmetingen. Hieronder zal een afschatting van die fout gegeven worden:

$\Delta p_x = 0.3987 * \Delta V_x \pm 0.0164$ mm

$\Delta p_y = 0.1219 * \Delta V_y \pm 0.0148$ mm

Het verschil in pixels is in beide richtingen ongeveer 365, $\Delta V_x \approx 2.86$ en $\Delta V_y \approx 6.46$ Volt zodat de breedte en hoogte 1 pixel zijn:

$b_p \approx 3.124$ μm
$h_p \approx 2.157$ μm

Tabel B4: *pixelgrootte in x- en y-richting*
De bijbehorende nauwkeurigheden zijn:

$f_{bp} = 4.5 * 10^{-2}$ μm
$f_{hp} = 4.1 * 10^{-2}$ μm

B.1.4 Meetnauwkeurigheid

Bij het bewerken van de videobeelden wordt eerst op t=0 sec een referentiepunt vastgesteld. Daarna worden op verschillende tijdstippen de verplaatsing van het zwaartepunt t.o.v. dit referentiepunt bepaald in pixels (Δp_x en Δp_y). De verplaatsingen in mm worden berekend door te vermenigvuldigen met de pixelbreedte cq hoogte:

$U_1 = \Delta p_x * b_p$

$V_1 = \Delta p_y * h_p$

De fout die kan optreden kan bepaald worden uit de fouten van de verschillende

onderdelen :

$$f_{totx} = \Delta p_x * f_{bp} + 2 * b_p * f_{tx} + f_{ux} = 0.045 * \Delta p_x + 0.687 + (0.0025 + 0.017 * \tan\varphi) * U_1$$

$$f_{toty} = \Delta p_y * f_{hp} + 2 * h_p * f_{ty} + f_{uy} = 0.041 * \Delta p_y + 0.345 + (0.00006 + 0.017/\tan\varphi) * V_1$$

Om tot een absolute waarde te komen geldende voor het hele meetgebied is deze vergelijking uitgewerkt voor de meting van de referentieconfiguratie als U_1 maximaal is: $\Delta p_x = 5.5$, $\Delta p_y = 19.4$ en $\tan\varphi = 2.5$ °, waaruit volgt;

$f_{totx} = 1.7$ µm
$f_{toty} = 1.4$ µm

B.2 Resultaten en aanbevelingen

In Figuur B5-B7 staan de verplaatsingsmetingen voor de verschillende configuraties tesamen met de verticale stempelverplaatsing bij een belasting van F=1.5 N. U_1 en V_1 geven de verplaatsing van de meniscus aan in respectievelijk x-en y-richting, V_2 is de stempelverplaatsing. Bij het aanbrengen van de belasting beweegt de meniscus naar buiten. Nadat de belasting is aangebracht wordt een teruggaande verplaatsing waargenomen en de uiteindelijke verplaatsing in x-richting is voor model A zelfs negatief.
Waarschijnlijk heeft er een extra rotatie plaatsgevonden van het speldje om de γ-as waardoor U_1 te klein en V_1 te groot wordt gemeten. Of er daadwerkelijk een rotatie heeft plaatsvindt is alleen te controleren als een tweede punt meegenomen wordt. Omdat de beeldgrootte maar 1 bij 1.5 mm was, zou dat twee (of meer) gaatjes binnen een afstand van minder als 1mm van elkaar betekenen wat met de huidige fabricage methode niet mogelijk was.
Een betere mogelijkheid zou wellicht zijn om de gehele of een gedeelte van de rand van de meniscus in beeld te nemen met een high definition camera.

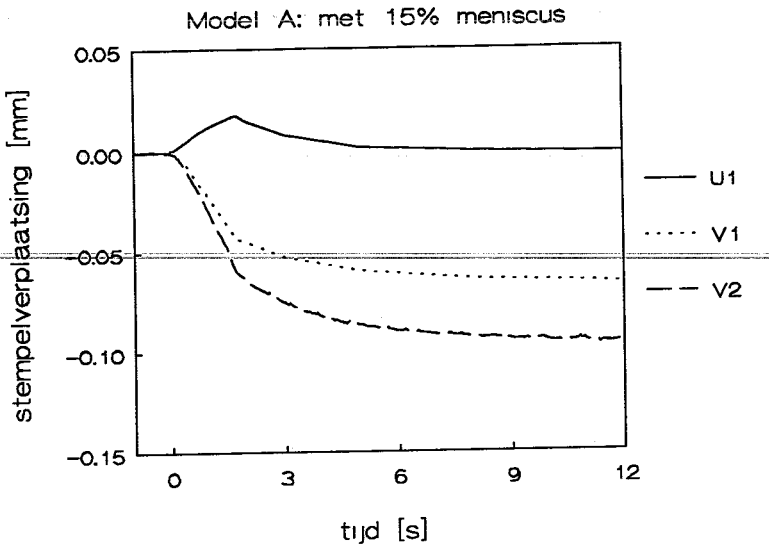

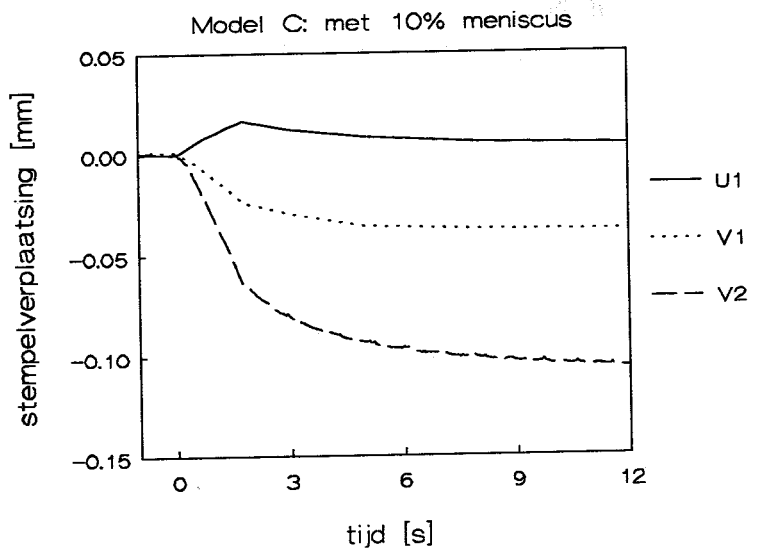

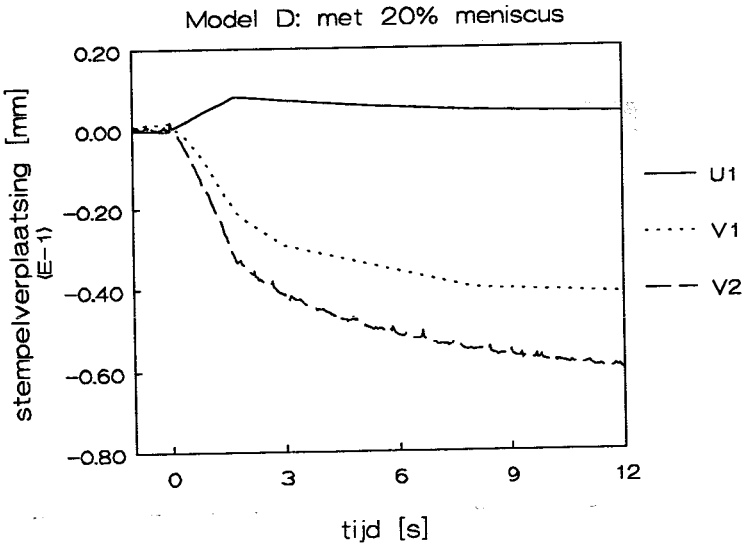

Figuur B5 tot B7: *Verplaatsing meniscus tesamen met stempelverplaating voor model A, C en D*

B.2 TIM-programma zpunt.cmd

```
;
;       zwaartepuntsbepaling van een rond gaatje:
;
/ini
/init
;       variabelen
int mnr
int pm
int pos
int am
int j
int var1
int var2
int px
int py
int xmin
int xmax
int ymin
int ymax
int yline
int nlines
int i
int summ
int cx1
int cx2
float z
float difcx
float midx
float xx
float yy
float totx
float toty
float cgx
float cgy
;
;       identificatie meting
;
cls
print "meting identificatie :"
mnr = "meting nummer ? "
pm = "percentage oplossing meniscus ? "
pos = "percentage oplossing poreuze schijf ? "
am = "aantal metingen ? "
fprint f:\b.m 0 "mnr = %u",mnr
fprint f:\b.m "\t % meting nummer\n"
fprint f:\b.m "pm = %u",pm
fprint f:\b.m "\t % percentage oplossing meniscus\n"
fprint f:\b.m "pos =%u",pos
fprint f:\b.m "\t % percentage oplossing poreuze schijf\n"
;
; aanmaken matrix met meetdata die later in matlab ingeladen kan worden
;
fprint f:\b.m "% kolom 1 = tijdstip, 2 = zpunt in x-richting, 3 = zpunt in y-richting\n"
fprint f:\b.m  "A = ["
;
;       een beeld wordt binnengehaald, opgedeeld in alleen
;       zwarte en witte pixels, de juiste marker wordt eruit gehaald en
```

```
;       daarvan het zwaartepunt bepaald
;
/init
while j < am
        cls
        era
        print "zoek het juiste beeld op en druk op een toets"
        set clock pll
        dig 0
        set clock xtal
        print "punt nr: ",j
        z = "tijdstip ?"
        thre 128
        bord 255
        ;
        ; bepaling goede marker
        ;
        label x
        var1 = 2
        var2 = mark var1
        while var2 < 400
                var1 = var1 + 1
                var2 = mark var1
        endw
        mark var1
        dis x
        ;
        ; window om marker heenleggen en randen bepalen
        ;
        px = cursx x
        py = cursy x
        xmin = px - 50
        xmax = px + 50
        ymin = py - 50
        ymax = py + 50
        nlines = ymax - ymin
        summ = 0
        i = 0
        totx = 0
        toty = 0
        while i <= nlines
                yline = ymin + i
                sgln x yline xmin yline xmax
                cx1 = cursx x
                sgln x yline xmax yline xmin
                cx2 = cursx x
                difcx = cx2 - cx1 + 1
                midx = cx1 + cx2 / 2
                if difcx > 0
                        xx = midx * difcx
                        yy = difcx * yline
                        totx = totx + xx
                        toty = toty + yy
                        summ = summ + difcx
                endif
                i = i + 1
        endw
        cgx = totx / summ
        cgy = toty / summ
```

```
            fprint f:\b.m "\n"
            fprint f:\b.m "%f",z
            fprint f:\b.m "\t"
            fprint f:\b.m "%f",cgx
            fprint f:\b.m "\t"
            fprint f:\b.m "%f",cgy
            beep
            j = j + 1
            print "zwaartepunt: x = ",cgx,", y = ",cgy
            pause
endw
fprint f:\b.m "];"
print "einde, vergeet niet de file te copieren !"
stop
```

Appendix C

Materiaal Karakterisatie

Ter karakterisering van de gebruikte materialen zijn schijven (afmetingen 52x10mm) aan een unconfined compression en een permeabiliteits proef onderworpen. Hiermee zijn een E-modulus en een permeabiliteit bepaald die als invoerparameters gebruikt zijn voor de numerieke berekeningen. Ook is nog een dwarscontractie coëfficient υ nodig, die genomen is uit trekproeven uitgevoerd op 10% trekstrippen, Goijaerts [5].

C.1 Drukproef

De drukproef is uitgevoerd met een Zwick trekbank. Een met olie doordrenkte schijf werd op een starre ondergrond geplaatst en met een platte plaat belast. Om te vermijden dat ook de olie voor krachtoverdracht zorgde is eerst het meeste uit de schijf geperst. Na initieel contact tussen plaat en schijf werd eerst een verplaatsing opgelegd van 0.5 mm om ervoor te zorgen dat het hele oppervlak van de schijf voor krachtdoorleiding zorgde. Hierna zijn 5 stappen van 0.2mm opgelegd. Na iedere stap is het materiaal 300 sec uitgerelaxeerd. 270 sec na oplegging van de verplaatsing zijn rekken en spanningen bepaald ervan uitgaande dat de schijf wrijvingsloos kon bewegen.
Er zijn twee schijven van 15% getest. Een was, net als de schijven van de andere oplossingen, direct in de juiste vorm gegoten. De ander was gesneden uit een 10 mm hoog blok materiaal. Figuur C1 laat de spanning vs rek zien voor de verschillende materialen en in Tabel C1 staan de elastische moduli die door deze punten gefit zijn(voor de 20% schijf is het laatste meetpunt niet meegenomen). De stijfheden van de 15% schijven verschillen een factor 2. Bij controle achteraf bleek in de eerste schijf gaten te zitten aan de buitenrand t.g.v. krimp van het materiaal. Gezien het feit dat de 10% en 20% schijven op dezelfde manier zijn gemaakt als 15%(1), kan er van uitgegaan worden dat dezelfde effecten in deze schijven optreden. Voor de experimenten is een 15% schijf gebruikt, gesneden uit een blok.

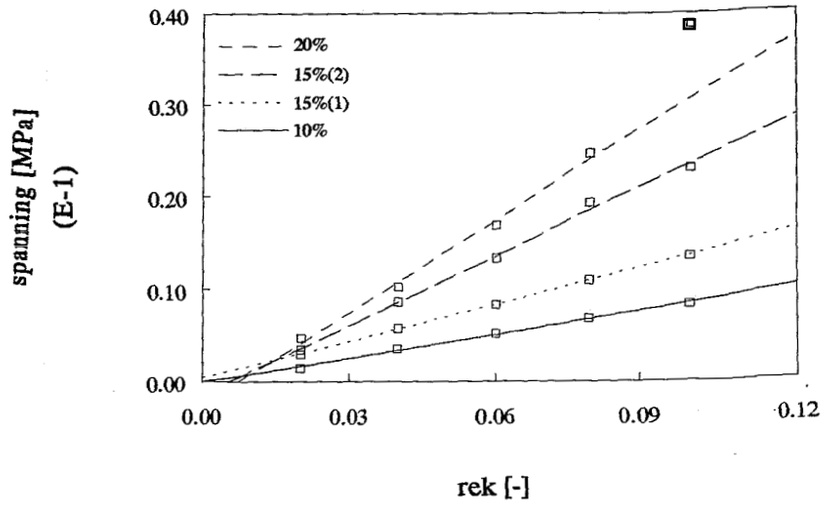

Figuur C1: *spanningen vs rek bepaald op 270 sec na aanbrengen stap*

materiaal	E (MPa)
10%	0.08
15% (1)	0.13
15% (2)	0.25
20%	0.33

Tabel C1: *E-moduli*

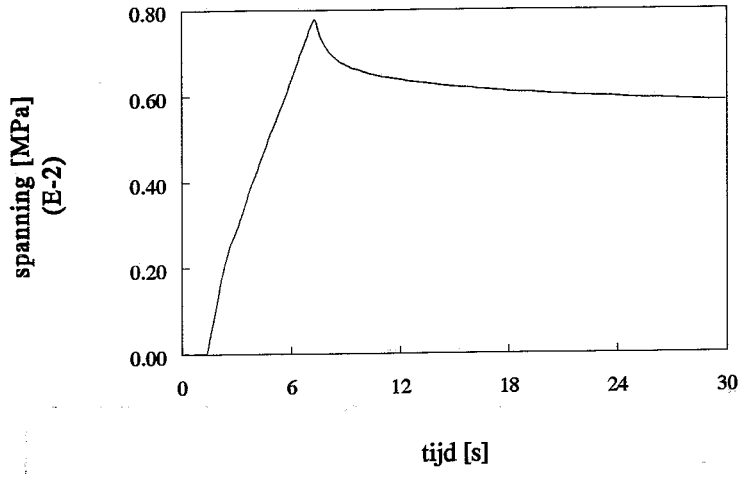

Figuur C2: *respons van 15% schijf (2) op een stap van 0.2 mm*

Figuur C2 laat de respons zien van de 15% schijf gedurende de eerste 30 sec na aanbrengen van een stap van 0.2 mm. Hieruit valt op te maken dat visco-elasticiteit een grote rol speelt en daarom is (handmatig) een 1-dimensionaal 3 parameter model gefit:

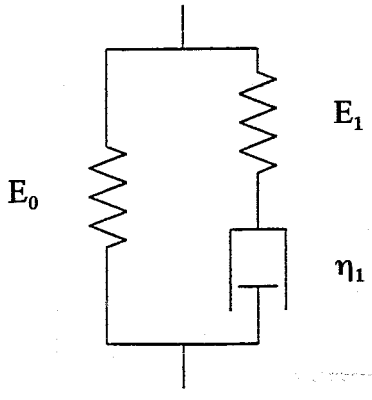

$E_0 = 0.3$ [MPa]

$E_1 = 0.2$ [MPa]

$\lambda_1 = \eta_1/E_1 = 1.7$ [s]

C.2 Permeabiliteit

C.2.1 Theorie

Omdat er weinig olie voorradig was, is een compacte opstelling ontworpen om de permeabiliteit te meten. Het ontwerp is te zien in Figuur C3. De buitenrand van de schijf word lichtjes geklemd tussen twee perspex bussen. Het midden van de schijf wordt ondersteund door een grof filter. Door de buis (d=10mm) met vloeistof te vullen wordt er een drukverschil aangebracht over het midden van de schijf (D=20mm). De vloeistof zal door het proefstuk gaan stromen en de kolom zal in hoogte afnemen. In tegenstelling tot conventionele opstellingen wordt het drukverschil dus niet constant gehouden, maar neemt af in de tijd. Hierdoor is de vloeistofsnelheid door het materiaal (q) in de wet van Darcy ook een functie van de tijd:

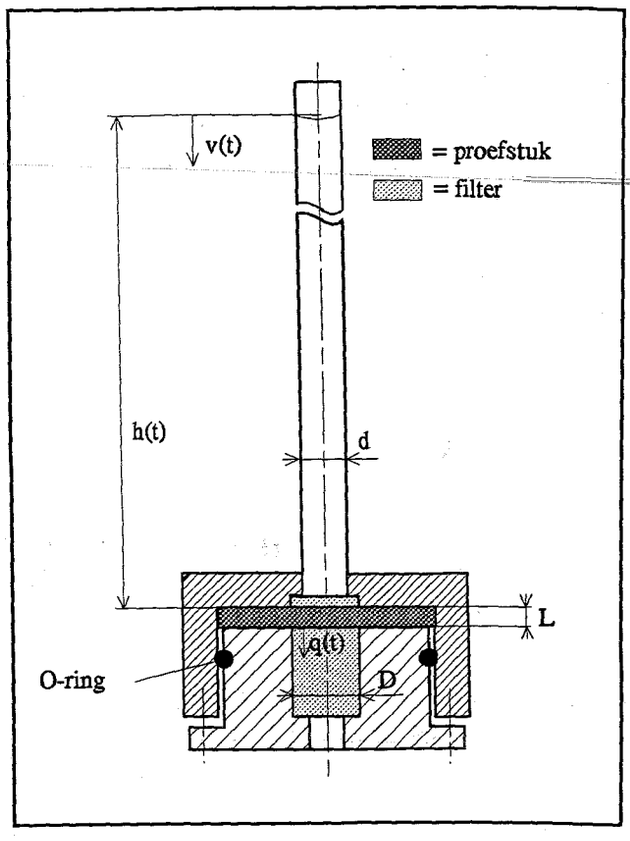

Figuur C3: *permeabiliteitsopstelling*

$$q(t) = -\frac{k}{L}\Delta p(t) \qquad (1)$$

Hierin is k de permeabilitiet, L de schijfdikte en Δp het drukverschil over de schijf. Voor de vloeistofstroming in de buis wordt uitgegaan van de Navier-Stokes vergelijking. Bij controle blijken visceuze, stationaire en instationaire krachten verwaarloosbaar en de volgende simpele krachtenbalans blijft over:

$$\Delta p(t) = \rho g h(t) \qquad (2)$$

met h de hoogte van de vloeistofkolom. Met de wet van behoud van massa vinden we een relatie tussen de snelheid van de vloeistof door het materiaal (q) en daalsnelheid van de vloeistofkolom (v):

$$v(t) = \frac{dh}{dt} = \frac{D^2}{d^2}q(t) \qquad (3)$$

Invullen van (1) en (2) in (3) levert:

$$v = \frac{dh}{dt} = \frac{1}{\rho g}\frac{d(\Delta p)}{dt} = \frac{D^2}{d^2}q = -\frac{D^2}{d^2}\frac{k\Delta p}{L} \qquad (4)$$

Voor het gemak is hier de tijdsafhankelijkheidsaanduiding achterwege gelaten. Dit resultaat kan omgeschreven worden met aan de ene kant alleen maar druktermen; integratie en invulling van (2) levert een formule voor de permeabiliteit:

$$k = -\ln\left|\frac{h_{t2}}{h_{t1}}\right| \frac{d^2 L}{D^2 \rho g (t_2 - t_1)} \qquad (5)$$

Als invoerparameters zijn dus twee vloeistofniveaus en bijbehorende tijdstippen nodig.

C.2.2 Experiment

De buis werd gevuld tot 1 meter boven het schijfoppervlak met olie. Om de 10 cm daling van de vloeistofkolom werd de tijd genoteerd en permeabiliteit bepaald, tot een hoogte van 50 cm was bereikt. Voor elke schijf is dit 5 keer gedaan, Figuur C4 en C5 laten de berekende permeabiliteiten zien als functie van de hoogte. De permeabiliteiten over de totale hoogteval zijn gemiddeld en staan in Tabel C3. De metingen werden gedaan bij een temperatuur van 21,5±1°C en de massadichtheid van de olie is $0.882*10^3$ kg/m^3.

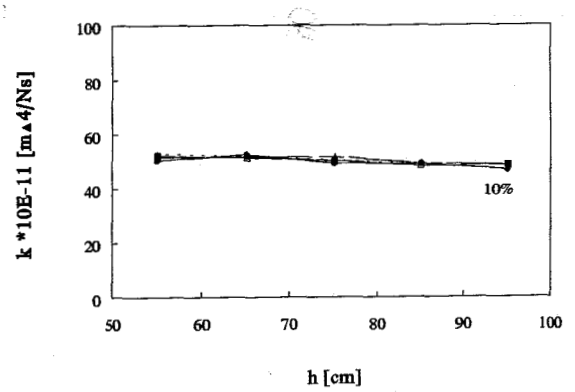

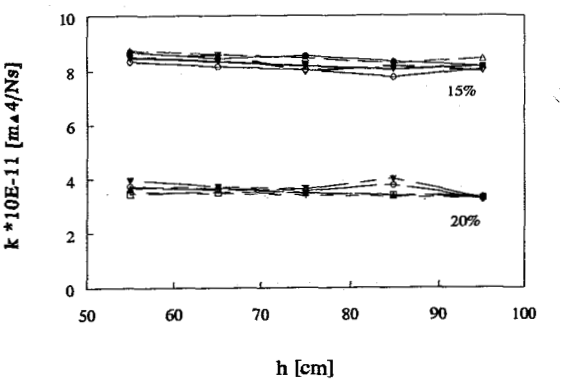

Figuur C4 en 5: *gemeten permeabiliteiten als functie van de hoogte van de vloeistofkolom voor resp. 10% materiaal en 15% en 20% materiaal*

materiaal	K [mm^4/Ns]
10%	510.2 ± 17.9
15%	84.1 ± 3.2
20%	33.2 ± 2.8

Tabel C3: *gemeten permeabiliteiten*

Bij de proeven zijn verschillende veronderstellingen gedaan, zoals geen wrijving tussen de platen en de schijf in de compression proef. In de permeabiliteitsproef is aangenomen dat vloeistofstroming door de buitenrand van de schijf geen rol speelt en dat de schijf aan de onderkant niet uitdroogt. Daarnaast dient nog opgemerkt worden dat de poriegrootte en daarmee ook permeabiliteit en stijfheid van het materiaal wordt bepaald door de snelheid waarmee de oplossing afkoelt. Daar deze niet goed controleerbaar is, leidt dit tot onzekerheid ten aanzien van reproduceerbaarheid, homogeniteit en isotropie van de schijven cq menisci. De gemeten E-moduli en permeabiliteiten kunnen dan ook niet gezien worden als meer dan een schatting en zijn dan ook op deze manier gebruikt.

Appendix D

Specificatie meetapparatuur

drukopnemers	: Philips KPZ20G
versterker	: Peekel-MCA100
AD-converter	: IDtech ADC488/8SA
verplaatsingsopnemers	: Scheavitz 050DC-D (W.F.W. 2331) Scheavitz 050HR-DC (W.F.W. 2384)
microscoop	: Questar QM100
camera	: HCS MXR
video	: Panasonic AG6200

Appendix E

Calibratie curves

E.1 drukopnemers

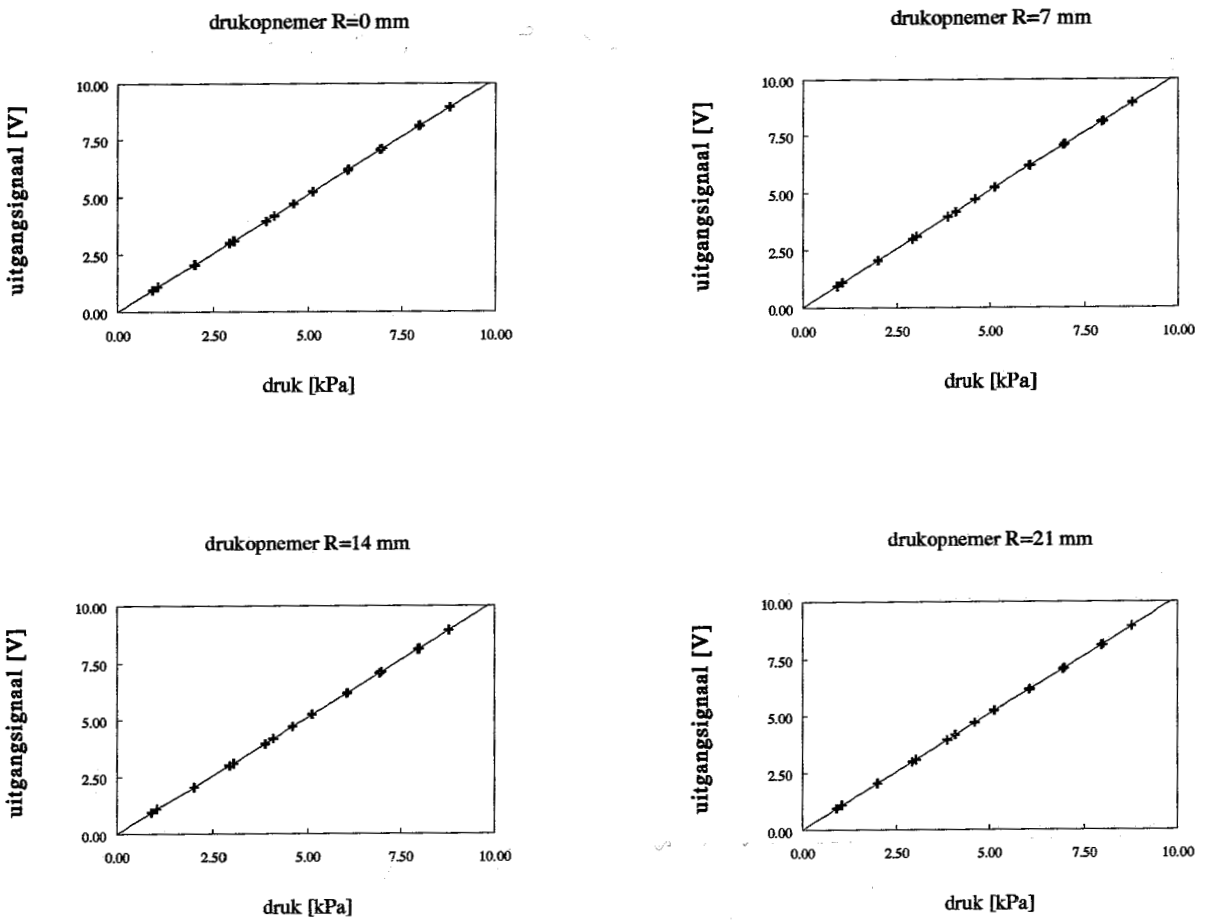

Figure E1-4: *Calibratie curves drukopnemers PHILIPS KPZ20G*

De drukopnemers zijn geijkt met een water manometer in een bereik van 0-10 kPa. Figuur E1-4 laten de ijkcurves zien en in Tabel E1 staan de gevonden relaties tussen in- en uitgangssignaal met de standaarddeviaties.

plaats drukopnemer	Δp/ΔV [-]	S [kPa]
R = 0	0.9824	0.0054
R = 7	0.9833	0.0060
R = 14	0.9831	0.0066
R = 21	0.9825	0.0063

Tabel E1: *karakteristieken drukopnemers*

Tijdens de experimenten is nog een verstoring op de signalen, veroorzaakt door andere apparaten, en een nulpuntsverschuiving waargenomen wat leidt tot de volgende nauwkeurigheid voor de drukopnemers:

P = 0.98*V ± 0.06 kPa

E.2 verplaatsingsopnemers

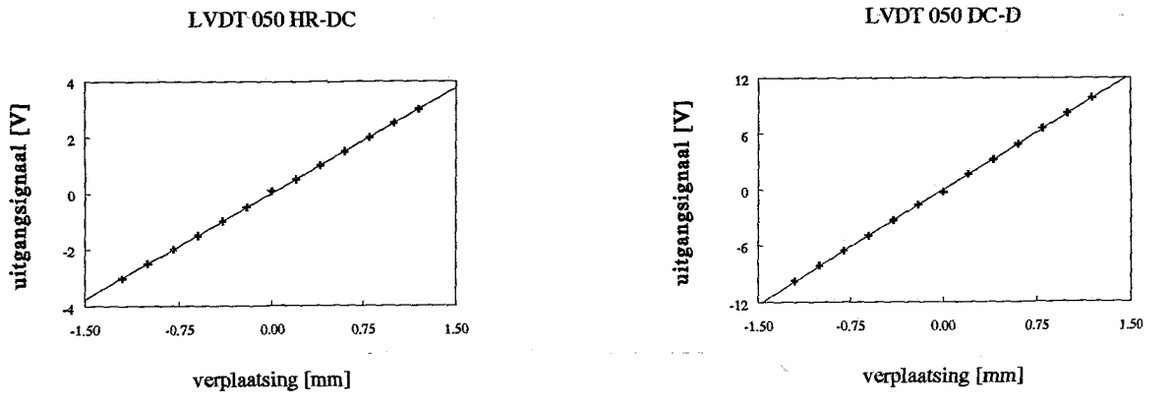

Figure E5-6: *Calibratie curves verplaatsingsopnemers*

In Figure E5-6 staan de ijkcurves van de verplaatsingsopnemers: Scheavitz 050HR-DC is gebruikt om de pixelgrootte in x-richting te bepalen en 050DC-D voor de pixelgrootte in y-richting en om de verticale verplaatsing van de stempel te meten. De verplaatsingsopnemers hebben de volgende nauwkeurigheid:

LVDT 050 DC-D : u = 0.1219*V ± 0.0074 mm LVDT 050 HR-DC : u = 0.3987*V ± 0.0082 mm

Appendix F

DIANA Programma's

In deze bijlage zijn de programma's opgenomen gebruikt in het software pakket DIANA. Voor de drie verschillende componenten waaruit het model bestond, te weten: schijf, meniscus en stempel, zijn eerst meshdata gegenereerd. Deze zijn samengevoegd in een nieuwe file tesamen met randvoorwaarden en materiaal grootheden. In overeenstemming met de experimenten is eerst de respons doorgerekend voor de voorbelasting. Daarna is een analyse uitgevoerd voor een belasting van 1.5 N.

F.1 Mesh generatie

SCHIJF.DAT :

```
data file 10mm dikke schijf

'MESH'
VERTICES DI=2
   1    0.0        0.0
   2   10.0        0.0
   3   10.0       10.0
   4    0.0       10.0
   5   20.0        0.0
   6   20.0       10.0
   7   26.0        0.0
   8   26.0       10.0
DIAGRAM
TOPOLOGY
   1  2
   4  3
DIVISION
   X  1.  (10) /
   Y  1.  (7) /
ELEMENTS Q8AXI
DIAGRAM
TOPOLOGY
   2  5
   3  6
DIVISION
   X  1.  (5) /
   Y  1.  (7) /
ELEMENTS Q8AXI
DIAGRAM
TOPOLOGY
   5  7
   6  8
DIVISION
   X  1.  (6) /
   Y  1.  (7) /
ELEMENTS Q8AXI
'END'
```

SCHIJF.COM :

```
commando file 10mm dikke schijf

*FILOS
INITIALIZE
*INPUT
*MESH
GENERA
END GENERA
INPUT FI= "schijf2.dat"
*END
*END
```

MEN.DAT :

```
data file meniscus

'MESH'
VERTICES DI=2
   1    10.0        10.0
   2    20.0        10.0
   3    10.0        11.71573
   4    15.2896     14.18861
   5    20.0        17.63932
DIAGRAM
TOPOLOGY
   1  m  2
   m  -  m
   3  4  5
DIVISION
   X  1.  (6) /
   Y  1.  (4) /
ELEMENTS Q8AXI
'END'
```

MEN.COM :

```
commando file meniscus

*FILOS
INITIALIZE
*INPUT
*MESH
GENERA
 PARAME SN=200 SE=200
END GENERA
INPUT FI= "men2.dat"
*END
*END
```

STEMP.DAT :

```
data file stempel (R=30mm)

'MESH'
VERTICES DI=2
   1     0.0        10.0
   2     4.0367     10.2728
   3     8.0        11.0863
   4    22.0        19.6039
   5    15.7644     14.4758
DIAGRAM
TOPOLOGY
   1  2  3
DIVISION
   X  1.   (8) /
ELEMENTS L4TRU
DIAGRAM
TOPOLOGY
   3  5  4
DIVISION
   X  1.    (10) /
ELEMENTS L4TRU
'END'
```

STEMP.COM :

```
commando file stempel

*FILOS
INITIALIZE
*INPUT
*MESH
GENERA
 PARAME SN=235 SE=235
END GENERA
INPUT FI= "stemp2.dat"
*END
*END
```

F.2 Analyses

TOT.DAT :

```
data file model F ; lineair elastisch, met meniscus, wrijvingsloos

'COORDINATES'
   1  0.000000E+00      0.000000E+00      0.000000E+00
   2  1.000000E+00      0.000000E+00      0.000000E+00
      ....................................
 252  2.087518E+00      1.843919E+00      0.000000E+00
 253  2.200000E+00      1.960390E+00      0.000000E+00
'ELEMENTS'
CONNECT
   1  Q8AXI   1 2 13 12
   2  Q8AXI   2 3 14 13
      ....................
 251  L4TRU   251 252
 252  L4TRU   252 253

:CONTACTELEMENTEN

 260  CNT2D 78 79 80 81 82 83 84 85
             235 236 237 238 239 240 241 242
 261  CNT2F 200 201 202 203 204 205
             87 88 124 125 126 127 128 171
 262  CNT2D 224 225 226 227 228 229
             244 245 246 247 248 249 250 251 252 253

MATERI
 / schijf_el / 1
 / meniscus_el / 2
 / stemp_el / 3
 / contact_el / 4
GEOMET
 / schijf_el / 1
 / meniscus_el / 2
 / stemp_el / 3
DATA
 / schijf_el / 1
 / meniscus_el / 2
 / contact_el1 / 3
 / contact_el2 / 4
 / contact_el3 / 5

'DIRECTIONS'
   1  1.000000E+00    0.000000E+00    0.000000E+00
   2  0.000000E+00    1.000000E+00    0.000000E+00
   3  0.000000E+00    0.000000E+00    1.000000E+00

'GROUPS'
ELEMEN
 1  schijf_el / 1-147 /
 2  meniscus_el / 200-219 /
 3  stemp_el / 235-252 /
 4  contact_el / 260-262 /
 5  contact_el1 / 260 /
 6  contact_el2 / 261 /
 7  contact_el3 / 262 /
```

```
: eenheden in N, mm, s

'MATERI'
1       YOUNG 0.4
        POISON 0.38
        PERMEA 22.5
        POROSI 0.85
2       YOUNG 0.4
        POISON 0.38
        PERMEA 22.5
        POROSI 0.85
3       YOUNG 1.E-6
4       ADHESI 1.

'GEOMET'
1       XAXIS 1. 0. 0.
2       XAXIS 1. 0. 0.
3       XAXIS 1. 0. 0.
        CROSSE 1.

'DATA'
1       MIXTUR
2       MIXTUR
3       NUMBER 8
4       NUMBER 6
5       NUMBER 6

'TYINGS'
EQUAL TR 2
/ 236-253 / 235

'SUPPORTS'
/ 1-11, 89-93, 129-134 / TR 1 TR 2
/ 235-253, 12-80(11) / TR 1
/ 81-87, 171-176, 134-170(6), 200-224(6), 205-229(6) / PR

'LOADS'
CASE 1
NODAL
235   FORCE 2 -1.25
'END'
```

TOT.COM :

```
commando file voorbelasting

*filos
 initia ma=20000
*input
*elasse
 store.x
*elmat
*loads
*solve me=iter
   perfor gmres mi=2000
   precon.r diagon
   check residu ep=1.D-8

*nonlin
initialize
 option nonsym tangen
 analys geomet dynamic
   use
     dampin.t
     backwd
   end use
 output neutra nosave
end initia
loadin
 load(1): (1) 1. /
```

```
  time 0.0:1.0 load(1) 0.0:0.0
  time 1.0:1.2 load(1) 0.0:1.0
  time 1.2:10.0 load(1) 1.0:1.000001
 end loadin

 select
  nodes 78-82 /
 end select
 output print
  force global residu
  displa total
 end output
 select
  nodes 1, 8, 90, 129 /
 end select
 output print
  presno total
 end output

 execute time steps
  size 1 0.001 0.009 0.04 0.05 0.3 0.6 0.8 /
  perfor newton regula mi=15
  solve me=iter
   prefor gmres mi=2000
   precon.r diagon
   check residu ep=1.D-8
  end solve
  norm refere energy
  norm check energy ep=1.D-3
 end execute steps

 execute time steps
  size 0.2 (2) 0.5 1.3 2.0 4.0 5.0 /
  perfor newton regula mi=10
  solve me=iter
   prefor gmres mi=2000
   precon.r diagon
   check residu ep=1.D-8
  end solve
  norm refere energy
  norm check energy ep=1.D-3
 end execute steps

 *end
 *end
```

TOT2.COM :

```
commando file belasting F=1.5 N

*nonlin
loadin
 time 16.0:17.72 load(1) 1.0:2.2
 time 17.72:35.0 load(1) 2.2:2.200001
end loadin

select
 nodes 78-82 /
end select
output print
 force global residu
 displa total
end output
select
 nodes 1, 8, 90, 129 /
end select
output print
 presno total
end output
```

```
select
  elemen schijf_el /
        nodes all /
  end elemen
end select
output neutra
      displa total
      presno total
      stress global cauchy
      strain global princi
end output

execute time steps
 size 0.001 0.009 0.09 0.15 (2) 0.2 (2) /
 perfor newton regula mi=15
 solve me=iter
  prefor gmres mi=2000
  precon.r diagon
  check residu ep=1.D-8
 end solve
 norm refere energy
 norm check energy ep=1.D-3
end execute steps

execute time steps
 size 0.5 0.3 0.1 0.02 (2) /
 perfor newton regula mi=15
 solve me=iter
  prefor gmres mi=2000
  precon.r diagon
  check residu ep=1.D-8
 end solve
 norm refere energy
 norm check energy ep=1.D-3
end execute steps

execute time steps
 size 0.26 0.5 1.0 1.5 (2) 2.5 3.0 /
 perfor newton regula mi=15
 solve me=iter
  prefor gmres mi=2000
  precon.r diagon
  check residu ep=1.D-8
 end solve
 norm refere energy
 norm check energy ep=1.D-3
end execute steps

*end
*end
```